Continuous Gravitational Waves

Takahiro S. Yamamoto (RESCEU U. Tokyo, Japan)

Winter School, 4 February 2026

Self-introduction

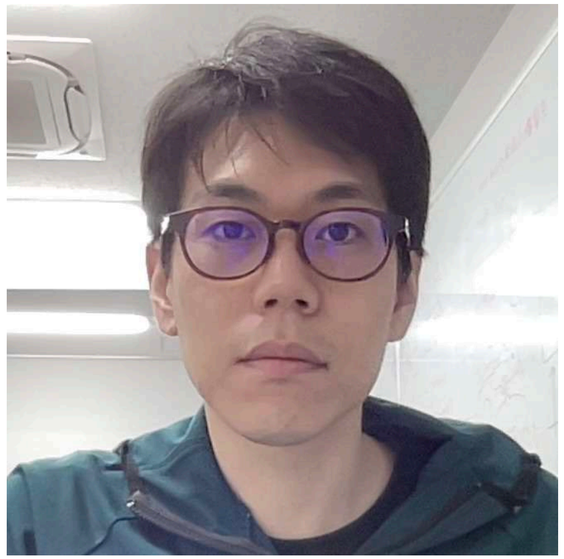

- Takahiro S. Yamamoto
- Project assistant professor
- RESCEU, University of Tokyo
- KAGRA member
  - Co-chair of continuous wave working group
  - Coauthor of KAGRA's "next 10 yr paper" [KAGRA, arXiv: 2508.03392]
- Research interest
  - Application of deep learning for GW data analysis
  - Ringdown GWs, continuous waves, popcorn background

Introduction

Gravitational waves = ripples of spacetime

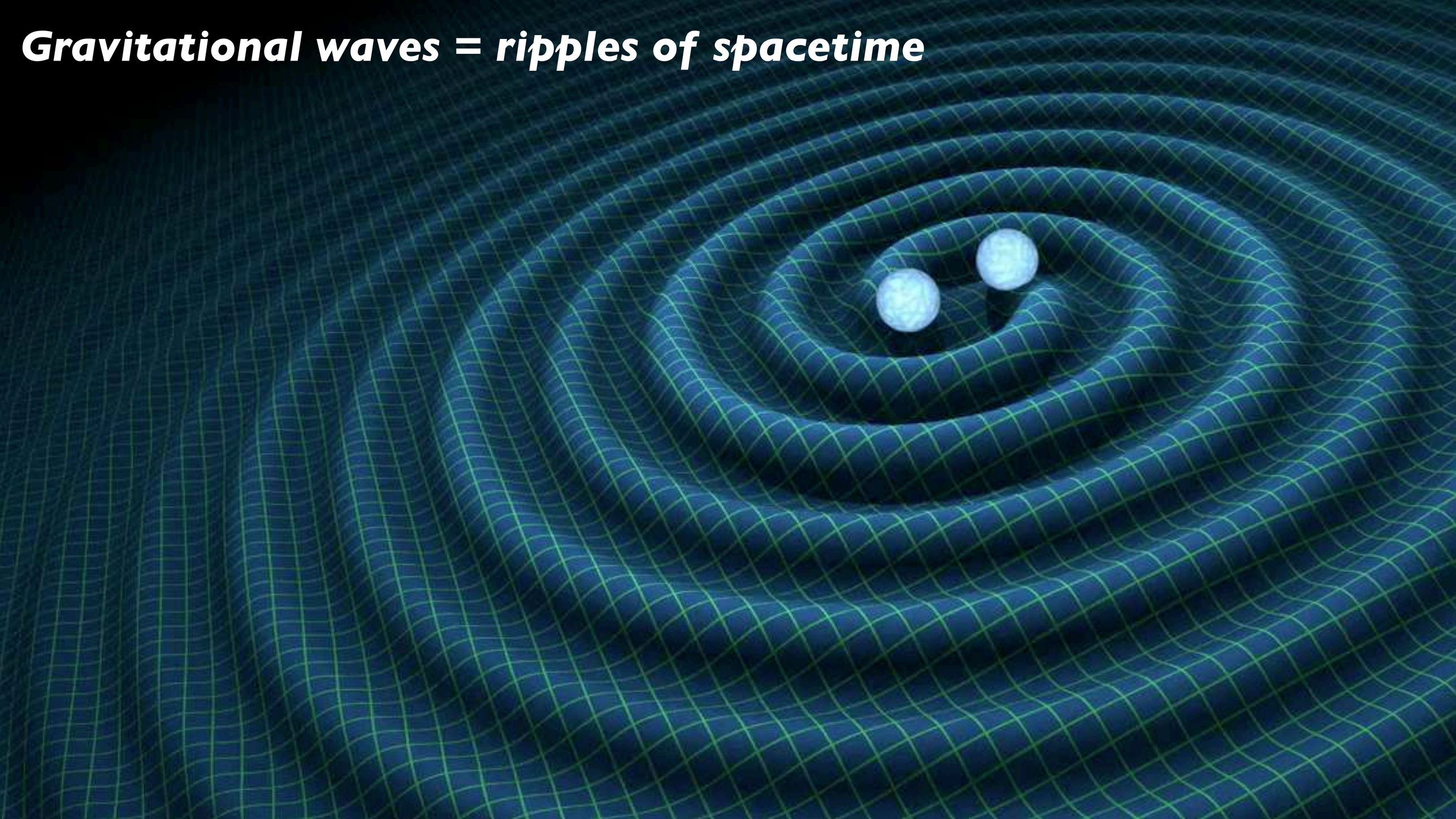

General relativity

cf. Pythagorean theorem

$s^2 = x^2 + y^2$

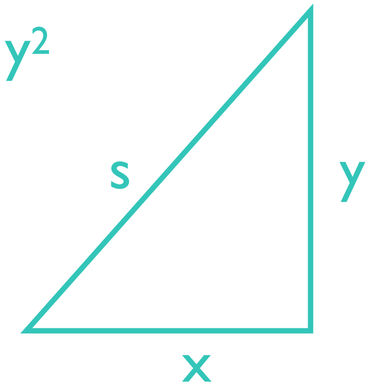

- Spacetime is dynamical.
- Infinitesimal distance $\mathrm{d}s^2 = g_{\mu\nu}\mathrm{d}x^\mu \mathrm{d}x^\nu$

Metric

Fundamental variable in GR

- Spacetime controls matter's motion/dynamics.
  Matter bends spacetime.

Einstein equation $G_{\mu\nu} = \dfrac{8\pi G}{c^4} T_{\mu\nu}$

$G_{\mu\nu}$: Einstein tensor

$T_{\mu\nu}$: matter's energy-momentum tensor

Linearized Einstein equation

Einstein equation $$G_{\mu\nu} = \frac{8\pi G}{c^4} T_{\mu\nu}$$

Perturbation on flat (Minkowski) spacetime

$$g_{\mu\nu} = \eta_{\mu\nu} + h_{\mu\nu}\,, \quad |h_{\mu\nu}| \ll 1$$

- Expand the Einstein equation up to 1st order of *h*

Linearized Einstein equation

$$\Box\psi_{\mu\nu} + \eta_{\mu\nu}\partial^\rho\partial^\sigma\psi_{\rho\sigma} - \partial_\mu\partial^\rho\psi_{\rho\nu} - \partial_\nu\partial^\rho\psi_{\mu\rho} = -\frac{16\pi G}{c^4} T_{\mu\nu}$$

$$\psi_{\mu\nu} := h_{\mu\nu} - \frac{1}{2} h\eta_{\mu\nu}$$

$$\Box := -\frac{1}{c^2}\frac{\partial}{\partial t^2} + \nabla^2$$

Lorentz gauge

- GR has general covariance: invariant under general coordinate transformations.
- You can choose gauge. Here, we apply the Lorentz gauge $\partial^\mu \psi_{\mu\nu} = 0$

Linearized Einstein equation with Lorentz gauge

$$\Box \psi_{\mu\nu} = -\frac{16\pi G}{c^4} T_{\mu\nu}$$

Transverse-Traceless (TT) gauge

- Consider the propagation of the perturbation (= gravitational waves) $\Box\psi_{\mu\nu} = 0$

- Lorentz gauge does not completely fix the gauge, so you can put an additional gauge.
  - Transverse $\partial^i \psi_{0i} = \partial^i h_{0i} = 0$
  - Traceless $\eta^{\mu\nu}\psi_{\mu\nu} = 0$

Linearized Einstein equation with TT gauge

$$\Box h_{ij}^{\mathrm{TT}} = 0 \qquad\qquad h_{00}^{\mathrm{TT}} = h_{0i}^{\mathrm{TT}} = 0$$

How many modes does GW have?

- e.g., Plane wave propagating along with z-axis $h_{ij}^{\mathrm{TT}} = A_{ij} e^{-i(\omega t - kz)}$

- TT gauge condition => $A_{iz} = 0\,, \quad A_{xx} + A_{yy} = 0$

$$h_{ij}^{\mathrm{TT}} = \begin{pmatrix} h_+ & h_\times & 0 \\ h_\times & -h_+ & 0 \\ 0 & 0 & 0 \end{pmatrix}_{ij} \times e^{-i(\omega t - kz)}$$

GW has 2 (tensor) modes. / Gravity has 2 dof.

Propagation of Gravitational waves

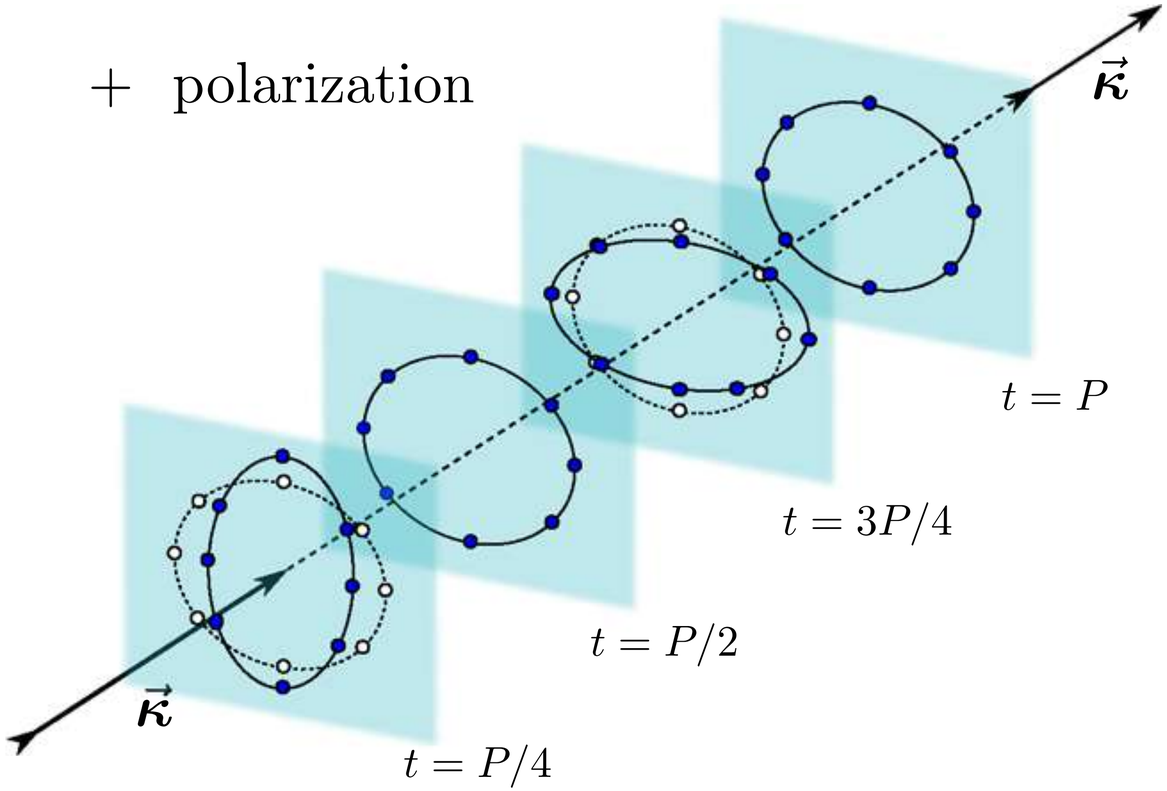

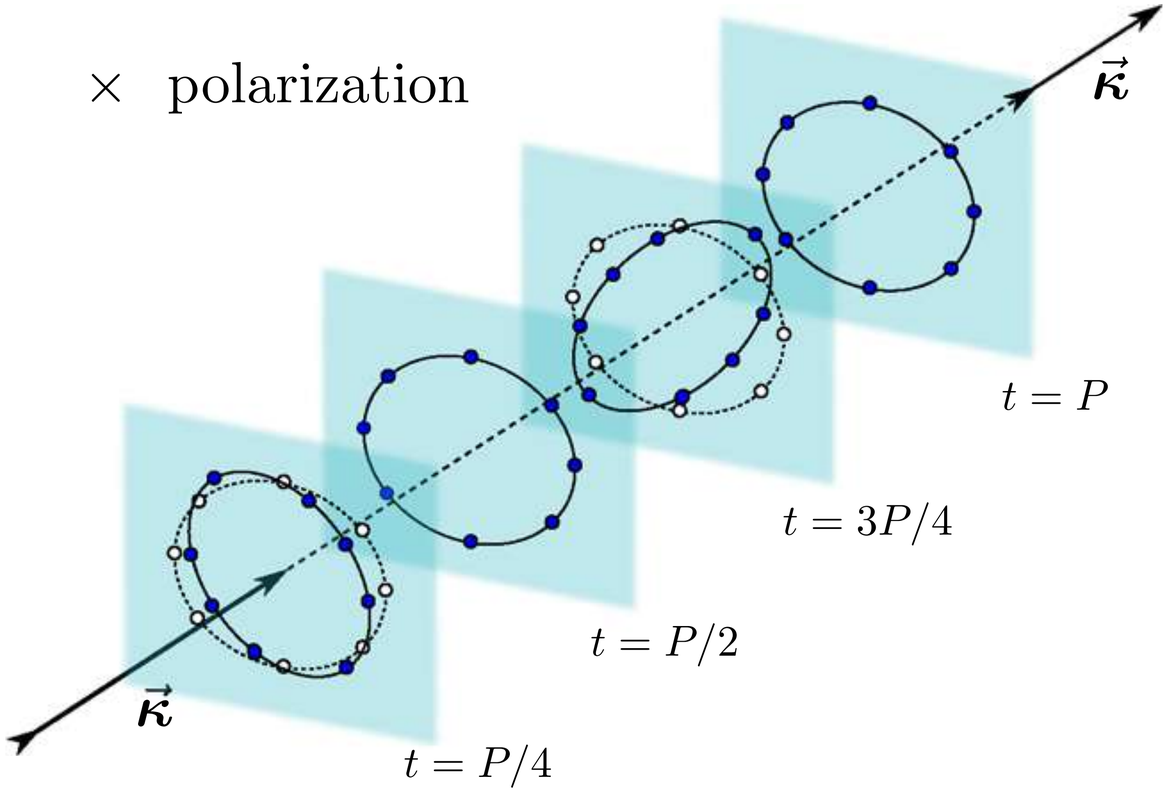

Fig. Bishop & Rezzola, Living Rev Relativ 19:2 (2016)

Generation of GWs

Wave equation with source term $\Box\psi_{\mu\nu} = -\dfrac{16\pi G}{c^4}T_{\mu\nu}$

- TT gauge condition
- Distant source, slow-motion approximation

$$\lambda, L \ll D$$

→ ***Multipole expansion***

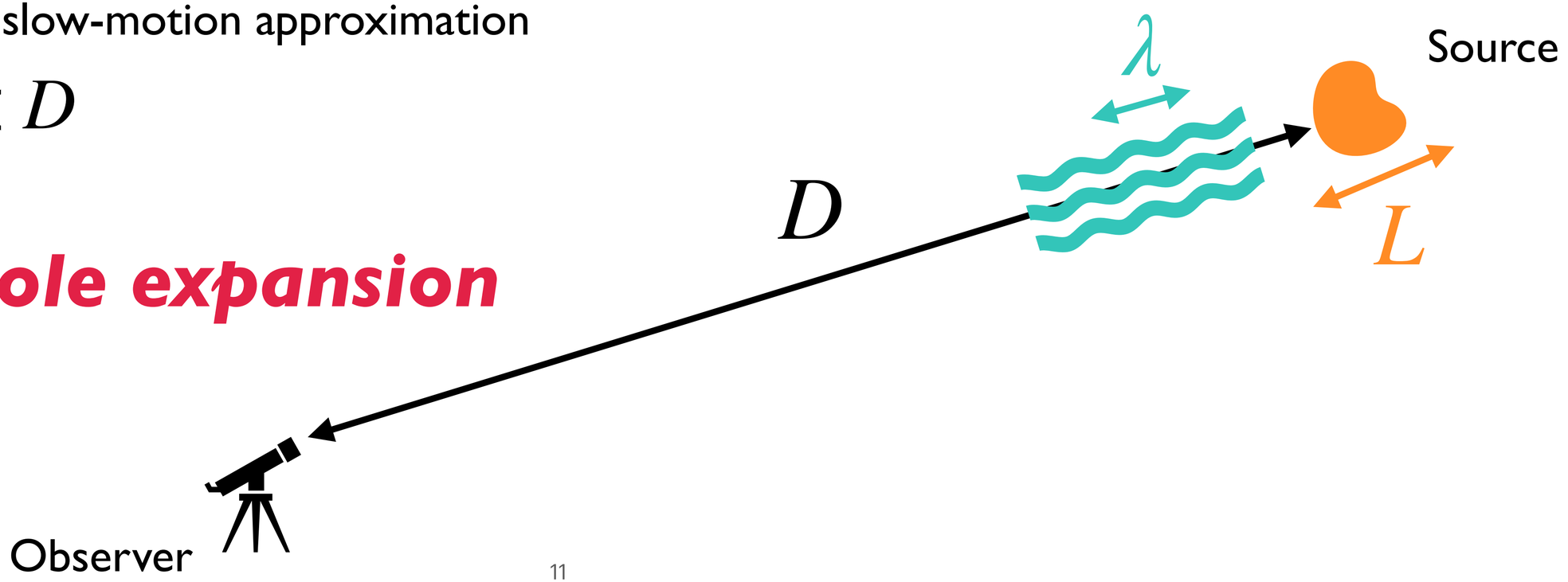

Generation of GWs

$$\Box\psi_{\mu\nu} = -\frac{16\pi G}{c^4}T_{\mu\nu}$$

- Solve the wave equation
- Taking the leading term of the multipole expansion.

Quadrupole formula

$$h_{ij}^{\mathrm{TT}}(t,\boldsymbol{x}) = \frac{1}{D}\frac{2G}{c^4}\frac{\mathrm{d}^2}{\mathrm{d}t^2}Q_{ij}(t-D/c)$$

cf., Electromagnetic waves

The leading term is dipole radiation.

$$Q_{ij} = \int \rho\cdot(x_i x_j - \frac{1}{3}x^2\delta_{ij})\mathrm{d}\boldsymbol{x}$$

Comparison with electromagnetic waves

	GWs	EM waves
Equation	$\Box\psi_{\mu\nu} = -\frac{16\pi G}{c^4}T_{\mu\nu}$	$\Box A_\mu = j_\mu$
Lorentz gauge	$\partial^\mu \psi_{\mu\nu} = 0$	$\partial^\mu A_\mu = 0$
Leading term of multipole expansion	quadrupole	dipole
Degree of freedom	2 polarization, transverse	2 polarization, transverse

GW Science

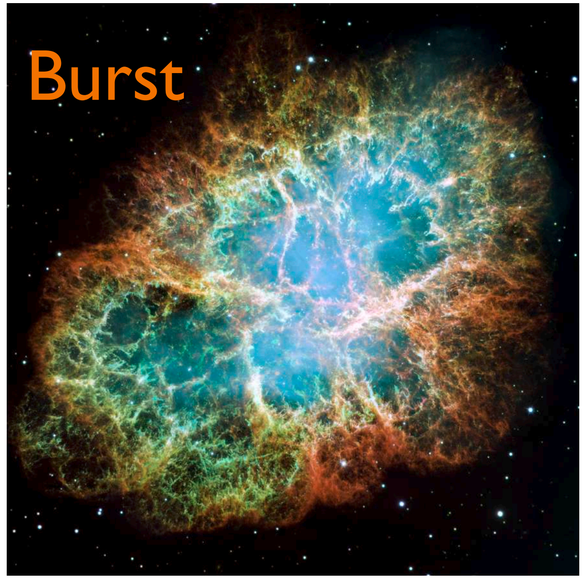

Credit: NASA

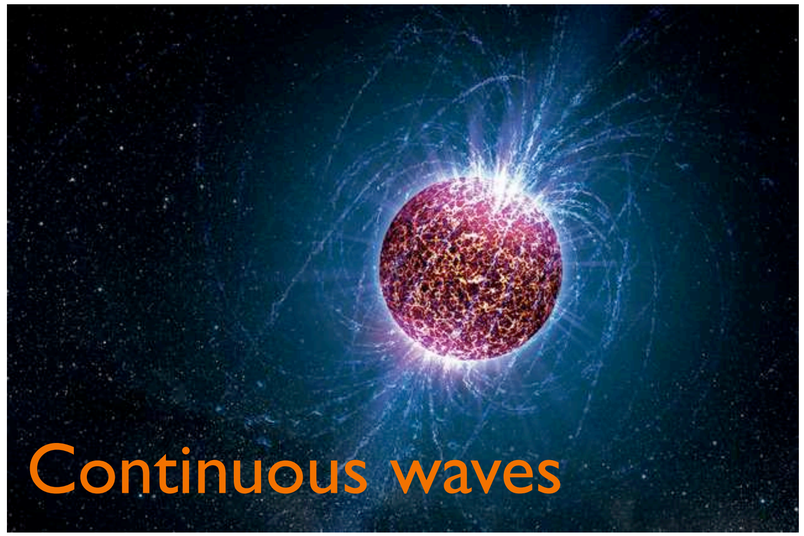

Credit: Casey Reed/Penn State University

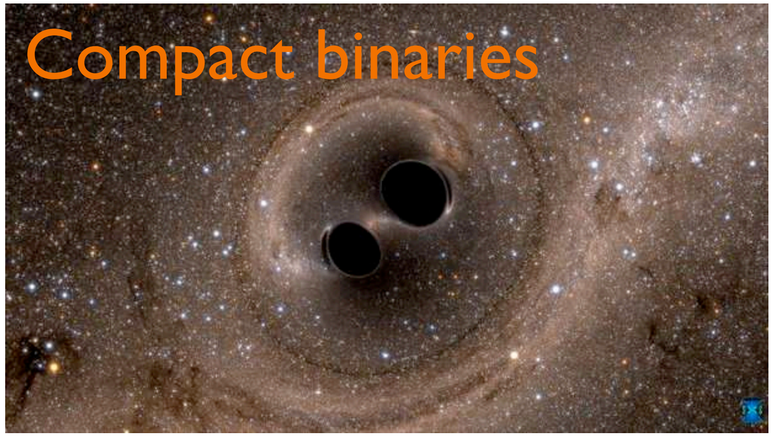

Credit: SXS project

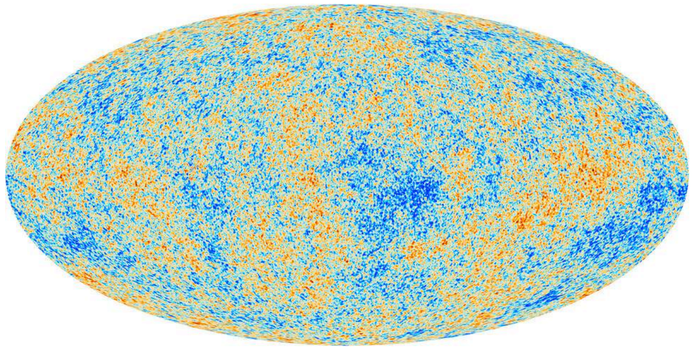

Stochastic background

Credit: ESA

- Astrophysics
  - Properties of compact objects (interior of NS, population, etc.)
  - Origin/mechanism of high-energy phenomenon
  - Multi-messenger observations
- Test of GR
- Cosmological implications

Laser interferometer as GW detectors

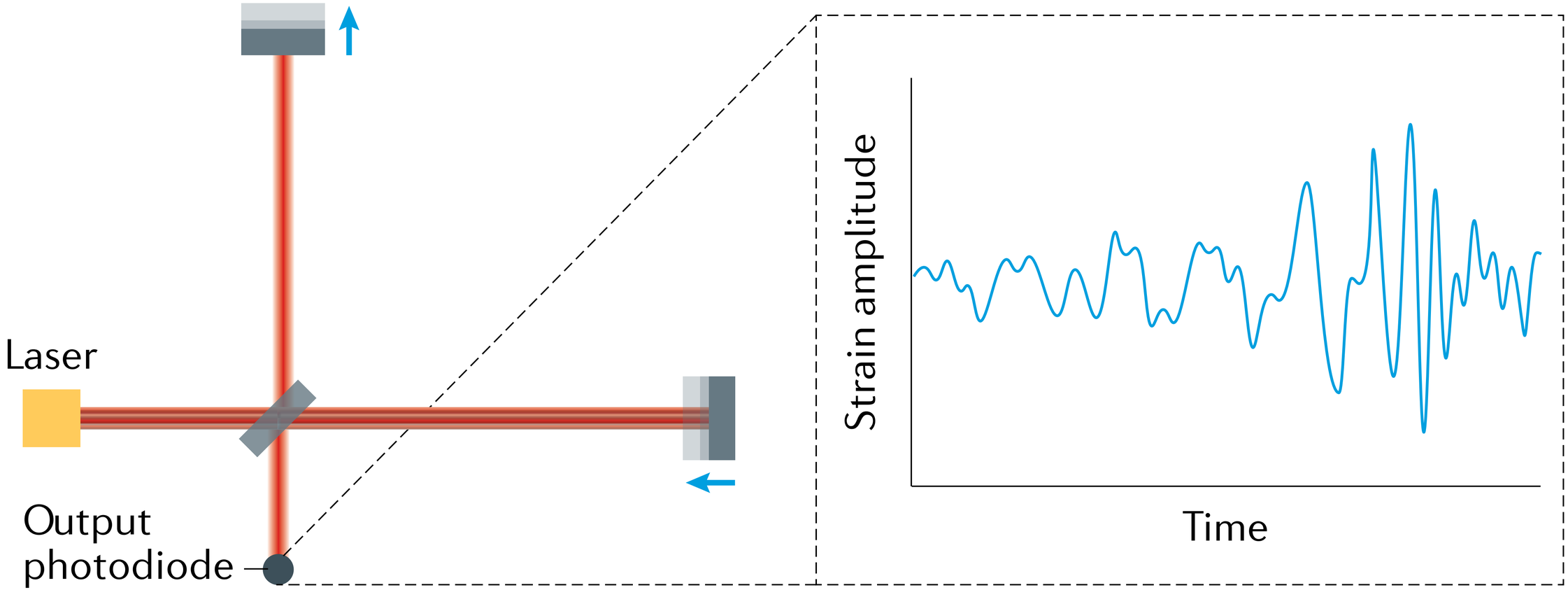

Fig. Bailes *et al.*, Nature Reviews Physics 3, 344 (2021)

Laser interferometers

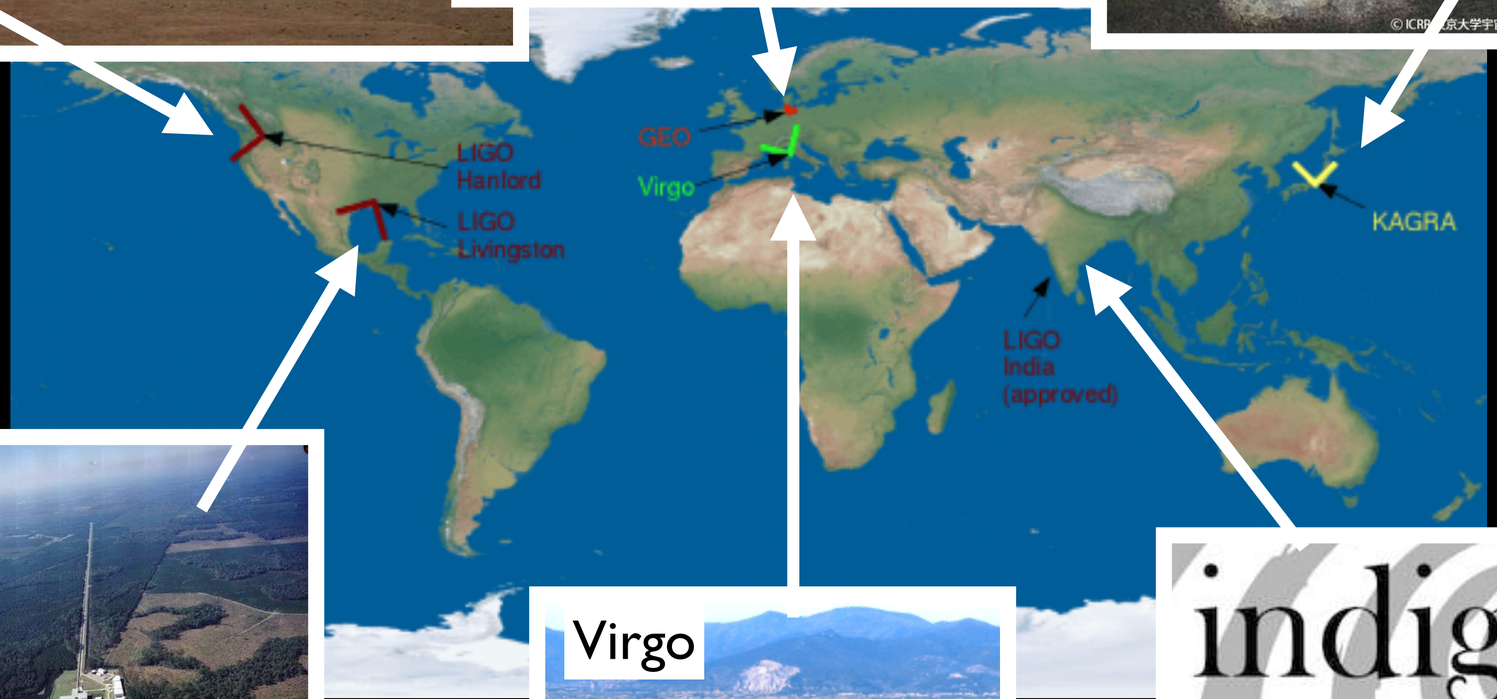

LIGO-India
(proposal)

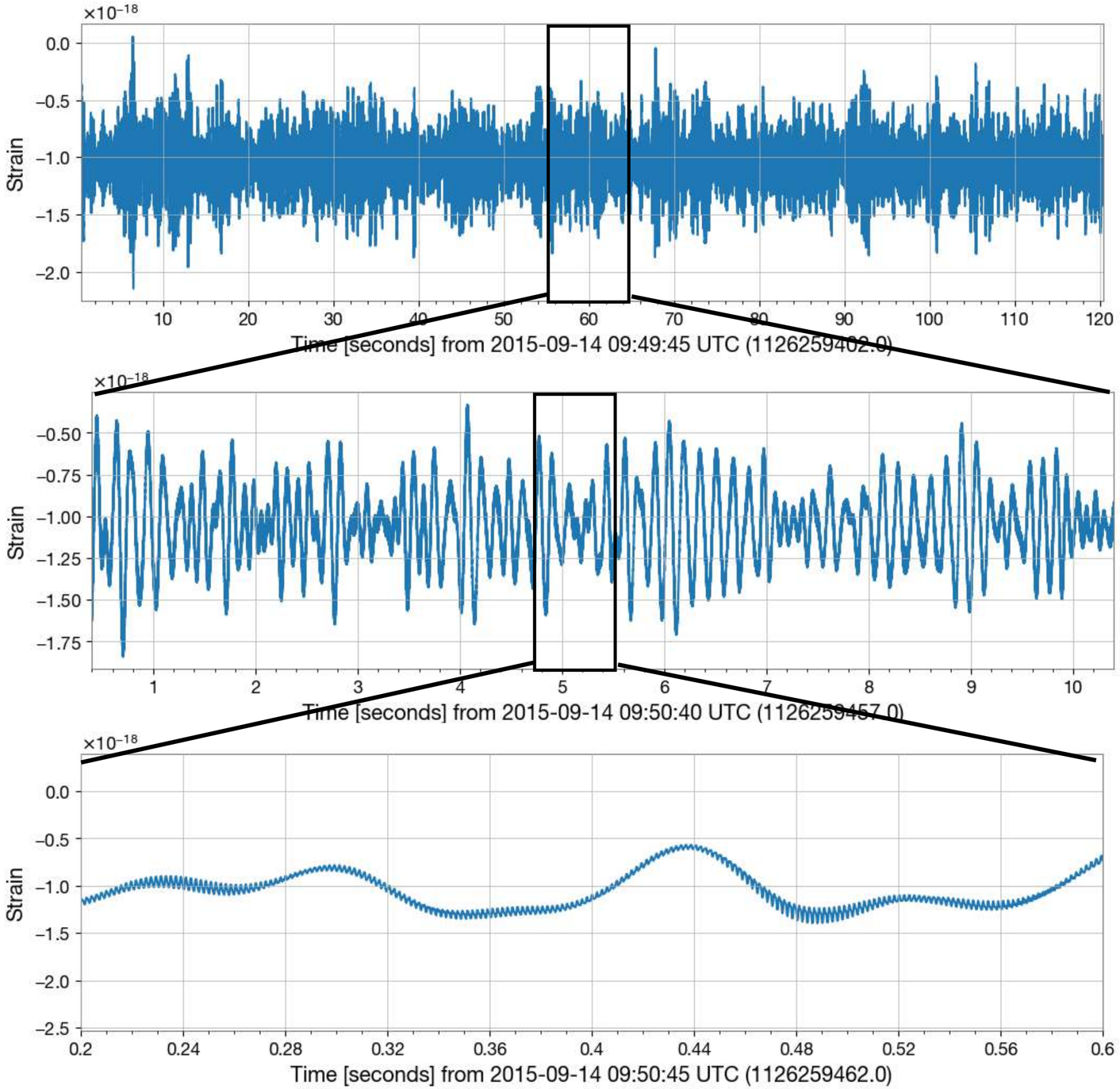
×10⁻¹⁸
Strain
Time [seconds] from 2015-09-14 09:49:45 UTC (1126259402.0)
Time [seconds] from 2015-09-14 09:50:40 UTC (1126259457.0)
Time [seconds] from 2015-09-14 09:50:45 UTC (1126259462.0)

120 s

10 s

0.4 s

LVK, (2025) ApJL995L18

Detector noise

- Detectors are contaminated by various noise (seismic, laser frequency, thermal, etc.)

- Power Spectral Density (PSD)

$$\langle \tilde{n}(f)\tilde{n}^*(f')\rangle = \frac{1}{2}S_{\rm n}(f)\delta(f-f')$$

- Current ground-based detectors are sensitive to 10~1000 Hz GWs.

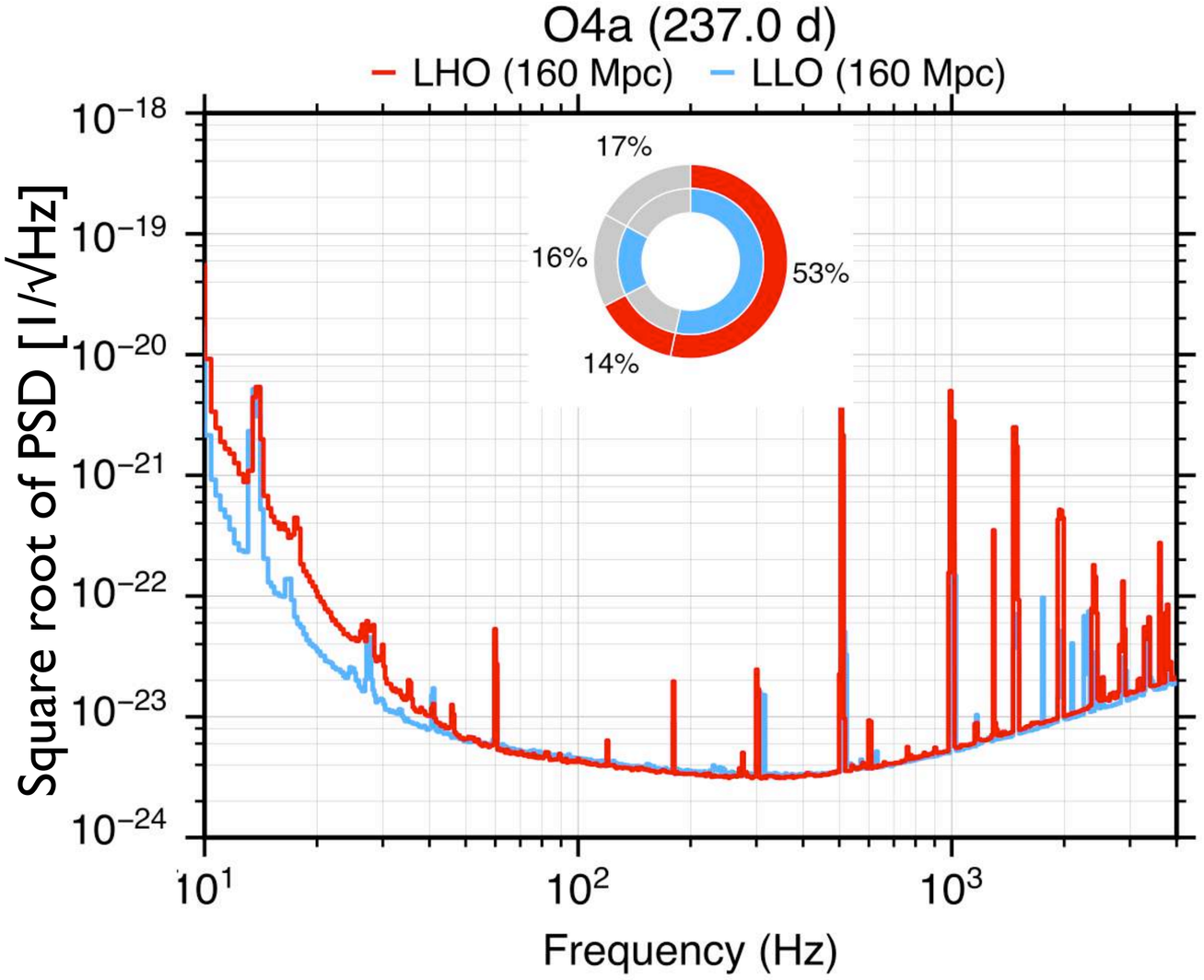

Continuous gravitational waves

CW sources

- ***CW = Continuous Waves = long-duration, quasi-monochromatic GWs***
- ***Rotating neutron stars, pulsars***
  - "mountain", r-mode, pulsar glitches, BNS remnants, X-ray binaries
  - Probing EOS of nuclear matter, dark population of NSs
- ***Exotic sources***
  - Boson cloud around rotating BHs
  - Planetary-mass PBH binary inspirals
  - Dark matter direct interaction

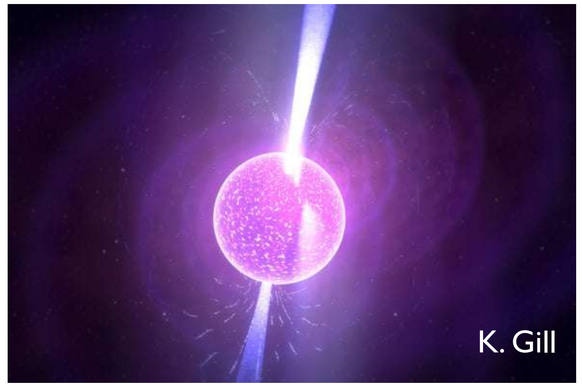

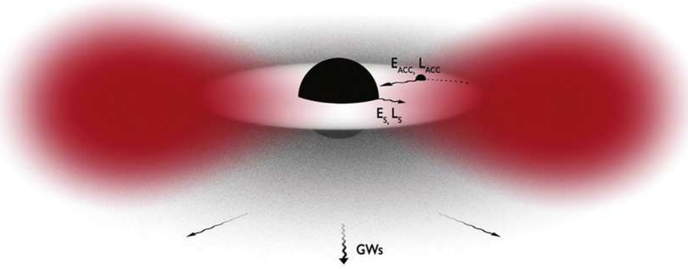

Brito *et al.*, Class. Quantum Grav. 32, 134001 (2015)

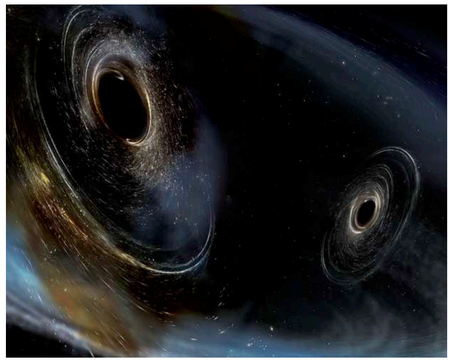

GWs from pulsars

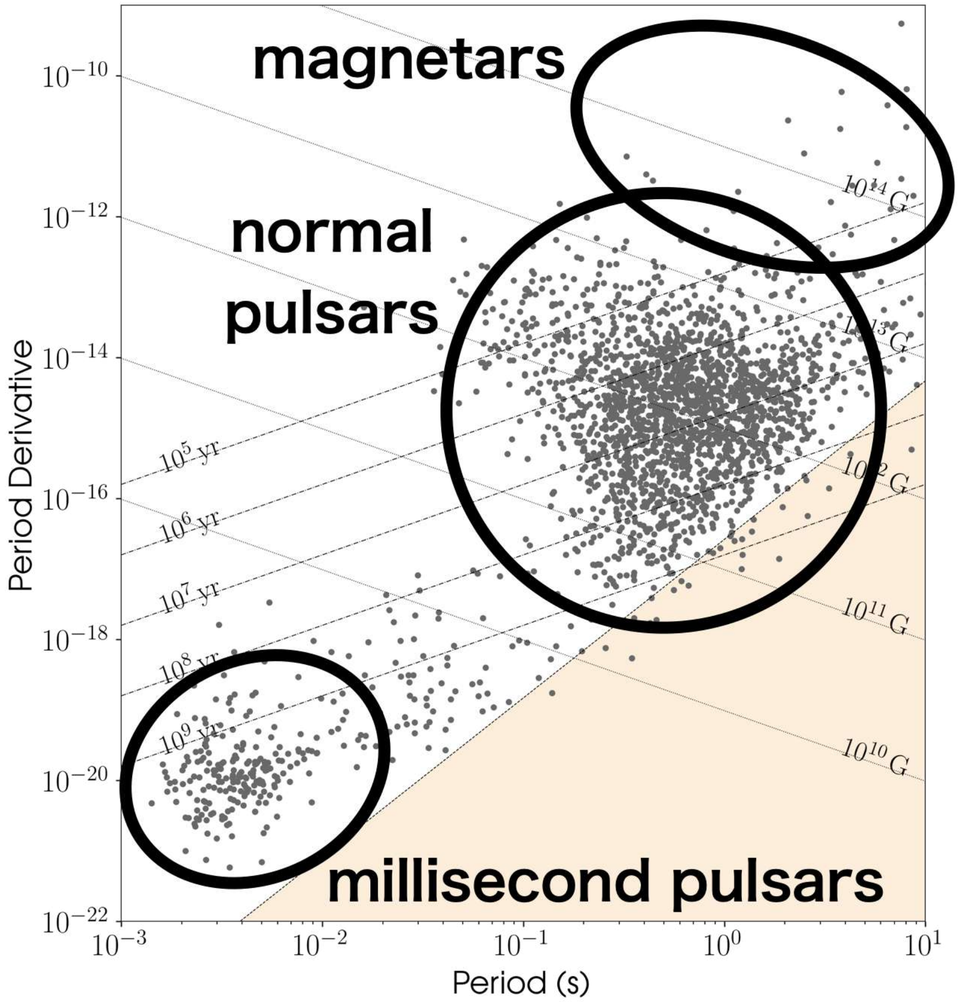

https://www.atnf.csiro.au/research/pulsar/psrcat/

Plotted by `psrqpy`

$$h_0 := \frac{4\pi^2 G}{c^4}\frac{Q_z f_{\rm gw}^2}{r}\epsilon$$

ellipticity $$\epsilon := \frac{Q_y - Q_x}{Q_z}$$

Q_x, Q_y, Q_z: NS's moment of inertia

Rough estimation

$$h_0 \simeq 10^{-26}\left(\frac{Q_z}{1.1\times 10^{45}\ \mathrm{g\ cm^2}}\right)\left(\frac{r}{1\mathrm{kpc}}\right)^{-1} \times \left(\frac{f_{\rm gw}}{100\ \mathrm{Hz}}\right)^2\left(\frac{\epsilon}{10^{-6}}\right)$$

Waveform model of CGWs

in source frame

τ : time when wavefront reaches at SSB (solar system barycenter)

Two polarizaion of GWs $h_+(\tau) = h_0 \cos[\Phi(\tau) + \Phi_0], h_\times(\tau) = h_0 \sin[\Phi(\tau) + \Phi_0]$

Phase of GWs $$\Phi(\tau) = 2\pi \sum_{k=0}^{s} \frac{f^{(k)}}{(k+1)!} (\tau - \tau_{\rm ref})^{k+1}$$

Frequency parameters $$f^{(k)} := \frac{d^k f}{d\tau^k}$$

At emission, the model of CGWs is simpler than those of CBCs.

Detector motion makes it complicated.

Waveform model of CGWs

in detector frame

1. Inclination angle

Amplitudes of +, x modes $h_+ \to h_0 \frac{1+\cos^2\iota}{2},\ h_\times \to h_0 \cos\iota$

2. Detector's antenna patterns

$$F_+(t;\alpha,\delta,\psi) = \sin\zeta\,[a(t;\alpha,\delta)\cos(2\psi) + b(t;\alpha,\delta)\sin(2\psi)]$$
$$F_\times(t;\alpha,\delta,\psi) = \sin\zeta\,[b(t;\alpha,\delta)\cos(2\psi) - a(t;\alpha,\delta)\sin(2\psi)]$$

ψ : polarization

ζ : Angle btw arms, π / 2 for LVK

3. Doppler modulation due to the detector motion

$$\tau = t - \frac{\boldsymbol{r}(t)\cdot\boldsymbol{n}(\alpha,\delta)}{c}$$

τ : SSB time, t : detector time

$\boldsymbol{r}(t)$: detector location with respect to SSB

$\boldsymbol{n}(\alpha, \delta)$: unit vector pointing from SSB to the source

What we will observe is

$$h(t) = F_+(t;\alpha,\delta,\psi)h_0\frac{1+\cos^2\iota}{2}\cos\left[\Phi(t) + \Phi_0\right] + F_\times(t;\alpha,\delta,\psi)h_0\cos\iota\sin\left[\Phi(t)+\Phi_0\right]$$

Frequency modulation

$$\Phi(\tau) = 2\pi \sum_{k=0}^{s} \frac{f^{(k)}}{(k+1)!} (\tau - \tau_{\mathrm{ref}})^{k+1}$$

$$\tau = t - \frac{\boldsymbol{r}(t) \cdot \boldsymbol{n}(\alpha, \delta)}{c}$$

$$f(t) = \frac{1}{2\pi} \frac{d\Phi}{dt}$$

$$\sim (f^{(0)} + f^{(1)} t + \cdots) \times \left(1 + \frac{\boldsymbol{v}(t) \cdot \boldsymbol{n}}{c}\right)$$

$$\sim \text{daily oscillation} + \text{yearly oscillation} + \text{intrinsic evolution}$$

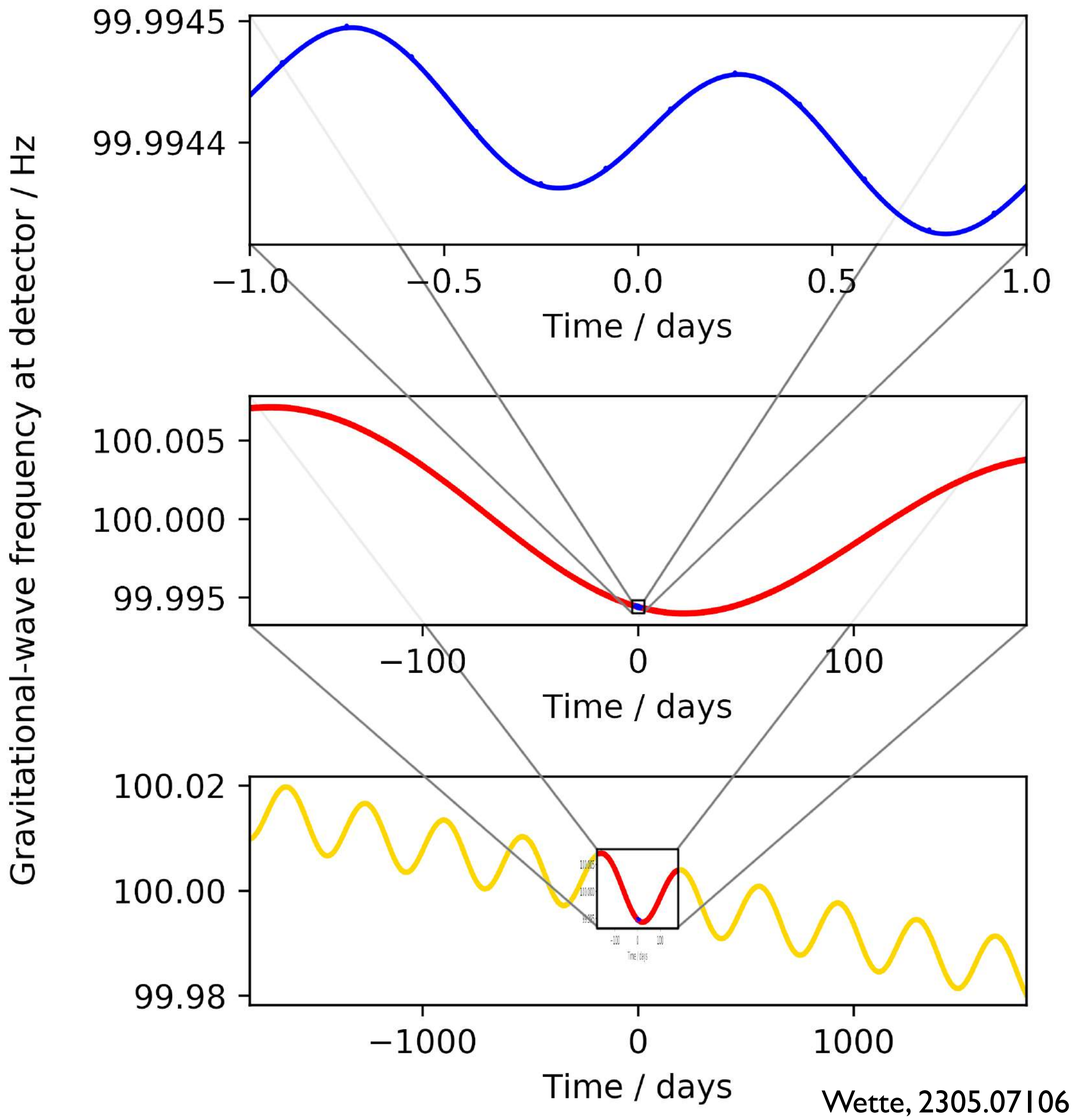

Wette, 2305.07106

CW searches

- ***CW detection is challenging.***
  - Amplitude is quite small ~ $O(10^{-26})$
  - Need to integrate O(yr) data
  - Large parameter space
  - ***# of templates can be $O(10^{18})$***
- ***Various types of search pipelines***
  - ***Targeted searches*** known [$f^{(0)}$, $\{f^{(k)}\}$, loc]
  - ***Directed searches*** known location
  - ***All-sky searches*** Unknown sources

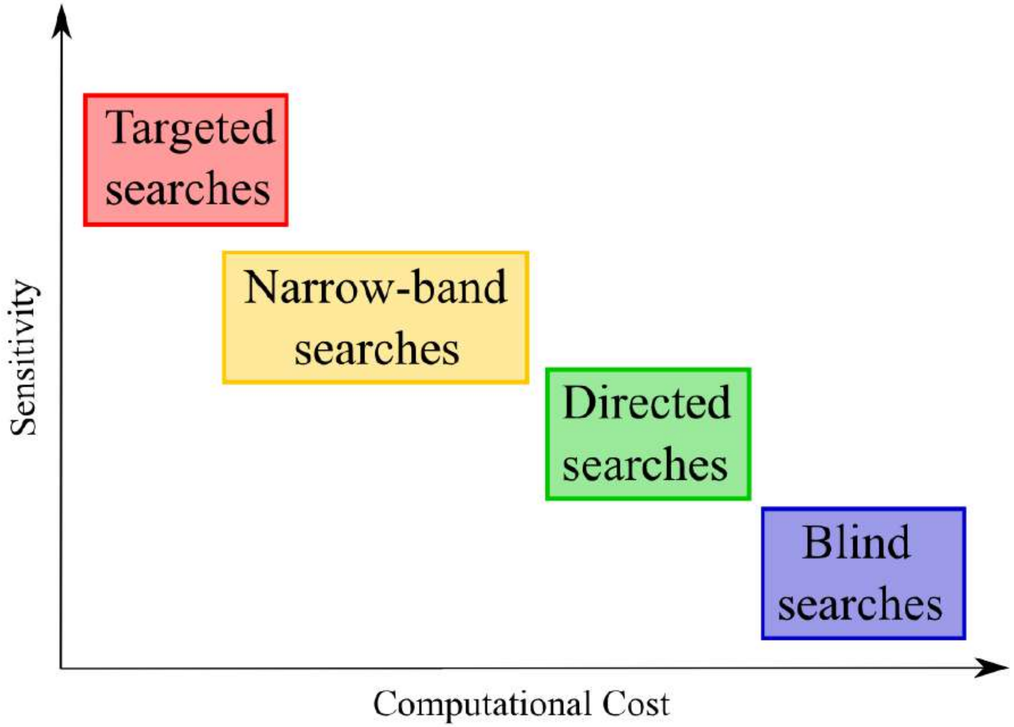

Fig. Sieniawska & Bejger, Universe 5(11), 217 (2019)

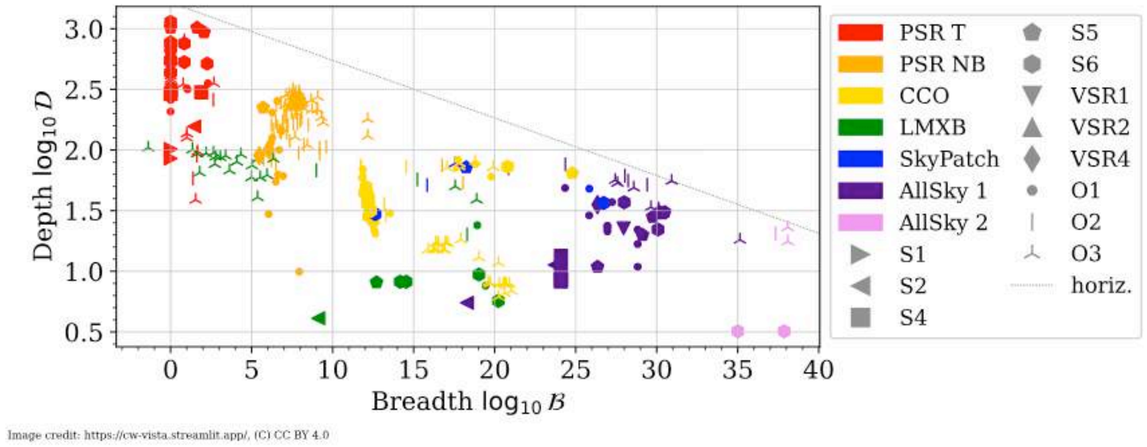

Web app "The CW Vista" by K. Wette

Difficulties in CGW searches

- **Non-Gaussian detector noise**

  There are two types of non-Gaussian detector noise; glitches and lines. They can affect the sensitivity by increasing the false-alarm rate and elevating the noise PSD.

- **Computational cost**

  Due to the long duration and the detector motion, CGW searches are quite sensitive to the small difference in the signal parameters. It leads to heavy computational cost.

Glitches

Glitches
= burst-like disturbances

Unlike CBC searches, glitches cannot be the sources of confusion with CGWs.

But, it affects the estimation of PSD by increasing noise floor.

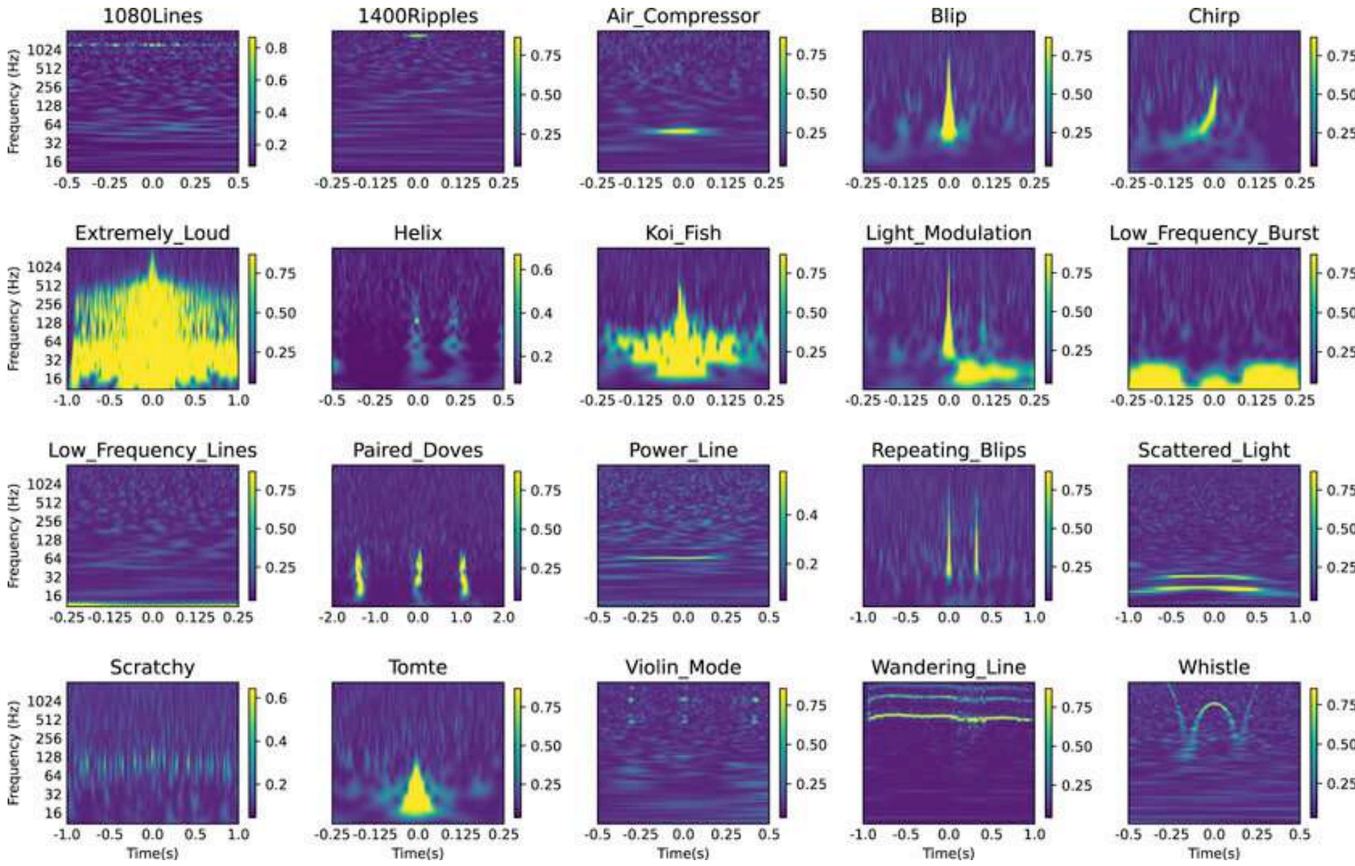

Instrumental lines

Instrumental lines
= narrow band, persistent artifacts

Sources:

- 60Hz power line harmonics,
- Violin modes of suspension
- Environmental disturbances, etc…

Instrumental lines can degrade the CW search sensitivity because they share the similar features with CGWs leading the increase of the false-alarm rate. Also, lines much affect on the PSD estimation.

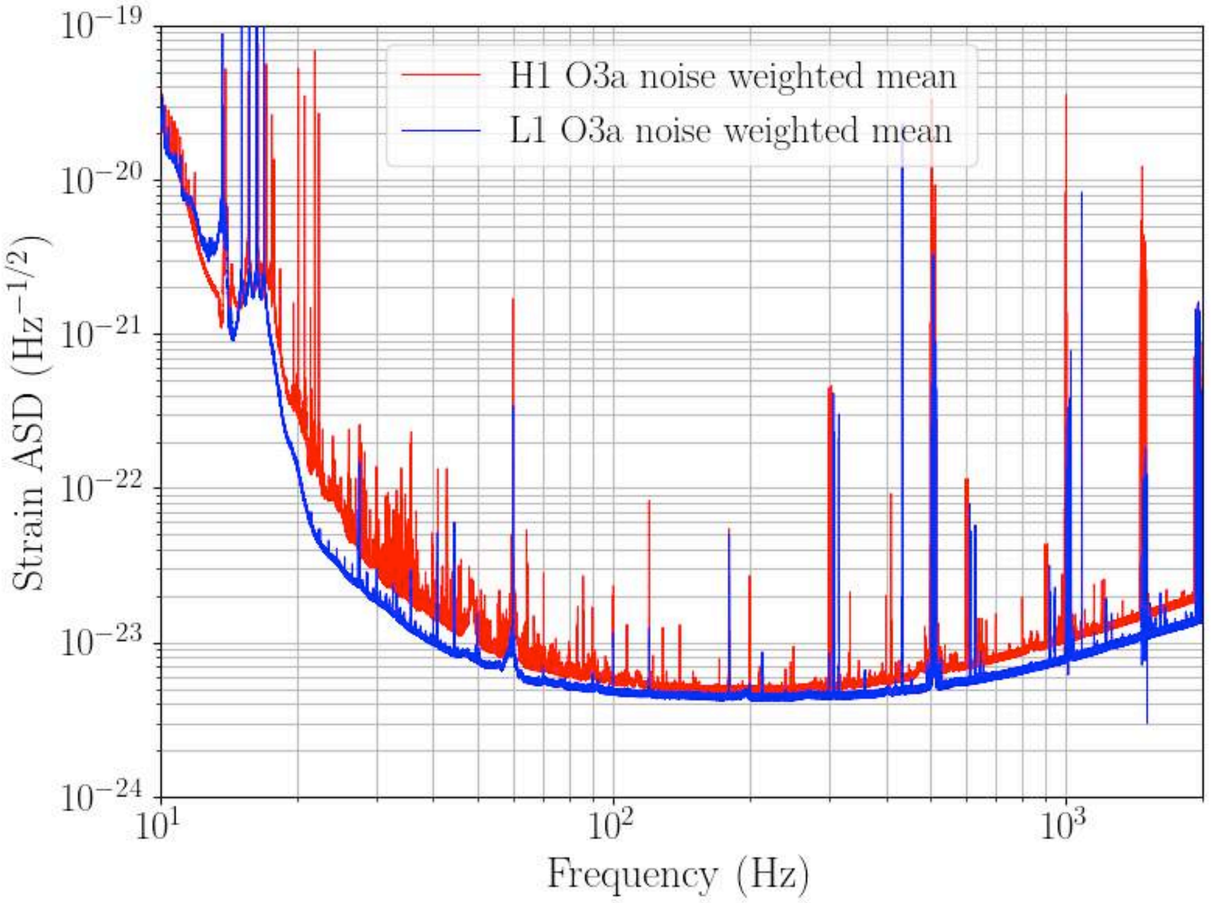

Fig: https://gwosc.org/O3/o3speclines/

$T_{\rm obs}$ dependency of computational cost

Idea: **difference in frequency should be smaller than $(T_{\rm obs})^{-1}$**

Resolutions $\Delta f^{(0)} \sim T_{\rm obs}^{-1}$ $\Delta f^{(1)} \sim T_{\rm obs}^{-2}$

$$\Delta\alpha \sim \Delta\delta \sim \left(f^{(0)}\frac{v}{c}\right)^{-1} \cdot T_{\rm obs}^{-1}$$

$$\text{Doppler modulation} \simeq f^{(0)}\frac{\boldsymbol{v}\cdot\boldsymbol{n}}{c}$$

$$\text{Small deviation} \sim f^{(0)}\frac{v}{c}\Delta\alpha \lesssim T_{\rm obs}^{-1}$$

Volume of the parameter space each grid covers $\Delta V_{\rm grid} \sim (T_{\rm obs})^{-5}$

Computational cost ~ (# of grids) x (comp. cost per grid) ~ $(T_{\rm obs})^{6}$

Long observational time leads to the rapid increase of the computational cost.

Semi-coherent searches

- Coherently processing entire observational data is not feasible. So, we divide it into short segments, process each segment coherently, and integrate them.
  Typically, T_{coh} = 1800 sec. But, it can be longer.

- The sensitivity is degraded comparing with the fully-coherent search. But, with the computational resource limitation, semi-coherent searches show better sensitivity than the coherent searches.

- Each algorithm returns candidates which satisfies the criteria and is followed by the follow-up search to confirm whether the candidates are astrophysical signals or detector artifacts.

Search pipelines employed in O3 all-sky searches

LVK collaboration, arXiv:2201.00697

- ***Time-domain F-statistic***

  Maximum likelihood based approach.

- ***Frequency Hough, sky Hough***

  Hough transform. Frequency Hough makes Hough map in ($f^{(0)}$, $f^{(1)}$) plane while sky Hough makes it in (α, δ) plane.

- ***PowerFlux***

  Adding SFT powers normalized by noise PSD and antenna pattern functions.

- ***SOAP-CNN***

  Combining Viterbi algorithm, machine learning technique to find the likely frequency track, and a convolutional neural network.

F-statistic

reference

Jaranowski, Królak, and Schutz, Phys.Rev.D58, 063001 (1998)

Multi-variate Gaussian distribution

- Multi-dimensional random variable $\mathbf{n} = (n_1, n_2, \cdots, n_d)$
- Gaussian distribution
  - $p(\mathbf{n}) \propto \exp\left[-\frac{1}{2} n_i (C^{-1})_{ij} n_j\right] , \quad (i, j = 1,2,\cdots, d)$
  - C is a covariance matrix

Matched filter

Notation *s(t)*: strain data, *h(t)*: GW waveform, *n(t)*: detector noise *n* = *s* + *h*

Assumption: detector noise is stationary and Gaussian with zero mean

Likelihood of *s(t)*

$$P(s|0) \propto \exp\left[-\frac{1}{2}(s|s)\right]$$ in the absence of signal

$$P(s|h) \propto \exp\left[-\frac{1}{2}(s-h|s-h)\right]$$ in the presence of signal

Log likelihood ratio

$$\ln \Lambda = \ln \frac{P(s|h)}{P(s|0)} = (s|h) - \frac{1}{2}(h|h)$$

noise-weighted inner product

$$(a|b) = 2\int_{-\infty}^{\infty} \mathrm{d}f \, \frac{\tilde{a}(f)\tilde{b}^*(f)}{S_\mathrm{n}(f)}$$

noise power spectral density (PSD)

$$\langle \tilde{n}(f)\tilde{n}^*(f')\rangle = \frac{1}{2}S_\mathrm{n}(f)\delta(f-f')$$

Difficulties in matched filtering

- Waveform model depends on various parameters
- You need to calculate matched filter SNR for every points in the parameter space
- The number of parameters is ~10, leading to the search over ~ 10 dimensional parameter space. This is a time-consuming task.

Rewrite signal model

- Parameters = { $f^{(0)}$, $\{f^{(k)}\}$, α, δ, h_0, ι, ψ, Φ_0 } 7+s parameters are too heavy.

Frequency evolution Amplitude

$$h(t) = F_+(t;\alpha,\delta,\psi)h_0\frac{1+\cos^2\iota}{2}\cos\left[\Phi(t)+\Phi_0\right] + F_\times(t;\alpha,\delta,\psi)h_0\cos\iota\sin\left[\Phi(t)+\Phi_0\right]$$

Antenna pattern functions

$$F_+(t) = \sin\zeta\left[a(t;\alpha,\delta)\cos(2\psi) + b(t;\alpha,\delta)\sin(2\psi)\right]$$
$$F_\times(t) = \sin\zeta\left[b(t;\alpha,\delta)\cos(2\psi) - a(t;\alpha,\delta)\sin(2\psi)\right]$$

$$h(t) = \sum_{\mu=1}^{4}\mathcal{A}^\mu(h_0,\iota,\psi,\Phi_0)h_\mu(t;f^{(0)},\{f^{(k)}\}\alpha,\delta)$$

F-statistic = likelihood ratio maximized over A^μ

Likelihood ratio can be rewritten by

$$\ln \Lambda = \mathcal{A}^\mu x_\mu - \frac{1}{2}\mathcal{A}^\mu \mathcal{M}_{\mu\nu}\mathcal{A}^\nu$$

Easily maximized over {Aμ}

with $x_\mu = (s|h_\mu),\ \mathcal{M}_{\mu\nu} = (h_\mu|h_\nu)$

Depending only on {$f^{(0)}$, {$f^{(k)}$}, α, δ}

F-statistic

$$2\mathcal{F} := \max_{\mathcal{A}} [\ln \Lambda] = x_\mu \mathcal{M}^{\mu\nu} x_\nu$$

$\mathcal{M}^{\mu\nu}$: inverse matrix of $\mathcal{M}_{\mu\nu}$

Using F-statistic, we can reduce the dimension of the parameter space by 4.

Statistics of F-statistic

F-statistic $2\mathcal{F} = x_\mu \mathcal{M}^{\mu\nu} x_\nu \sim Z_1^2 + Z_2^2 + Z_3^2 + Z_4^2$

In the absence of signal, 2*F* follows χ^2 distribution with 4 d.o.f

$$\mathbb{E}[2\mathcal{F}|0] = 4\,,\ \mathrm{Var}[2\mathcal{F}|0] = 8$$

If signal exists, 2*F* follows non-central χ^2 distribution

with 4 d.o.f and non-centrality of (h|h)

$$\mathbb{E}[2\mathcal{F}|h] = 4 + (h|h)\,,\ \mathrm{Var}[2\mathcal{F}|h] = 8 + 4(h|h)$$

$$\mathrm{SNR} = \frac{\mathbb{E}[2\mathcal{F}|h] - \mathbb{E}[2\mathcal{F}|0]}{\sqrt{\mathrm{Var}[2\mathcal{F}|0]}} = \frac{(h|h)}{2\sqrt{2}}$$

Semi-coherent F-statistc

Divide data into *N* segments and sum all F-statistics over all segments $2\mathcal{F}_{\rm tot} = \sum_{\ell=1}^{N} 2\mathcal{F}_{\ell}$

In the absence of signal, 2*F* follows χ^2 distribution with 4*N* d.o.f

$$\mathbb{E}[2\mathcal{F}_{\rm tot}|0] = 4N\,,\ \mathrm{Var}[2\mathcal{F}_{\rm tot}|0] = 8N$$

If signal exists, 2*F* follows non-central χ^2 distribution

with 4*N* d.o.f and non-centrality of (h|h)

$$\mathbb{E}[2\mathcal{F}_{\rm tot}|h] = 4N + (h|h)\,,\ \mathrm{Var}[2\mathcal{F}_{\rm tot}|h] = 8N + 4(h|h)$$

$$\mathrm{SNR}_{\rm semi} = \frac{\mathbb{E}[2\mathcal{F}_{\rm tot}|h] - \mathbb{E}[2\mathcal{F}_{\rm tot}|0]}{\sqrt{\mathrm{Var}[2\mathcal{F}_{\rm tot}|0]}} = \frac{(h|h)}{2\sqrt{2N}} = \mathrm{SNR}\cdot\frac{1}{\sqrt{N}}$$

This is an another explanation why semi-coherent search lose sensitivity.

But, under the limit of computational resources, it is not the case.

Frequency Hough

reference

Antonucci *et al.*, Class.Quant.Grav.25:184015,2008 (2008)

Astone *et al.*, Phys.Rev.D90, 042004 (2014)

Peak map

First of all, we make a periodogram and normalize it by noise PSD.

A pixel of the normalized periodogram is classified as a peak if a pixel satisfies two criteria:

(1) the power exceeds the given threshold, and (2) it is a local maxima.

Each pixel in a peak map has a value {0, 1}.

(Only noise)

Normalized power

for one SFT segment

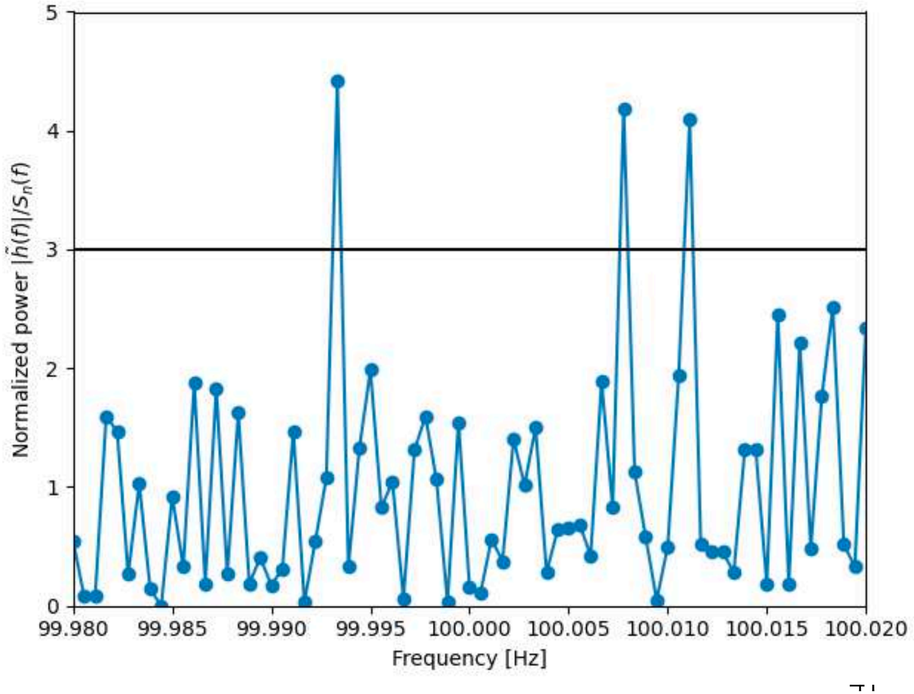

Peak map

Yellow: 1

Purple: 0

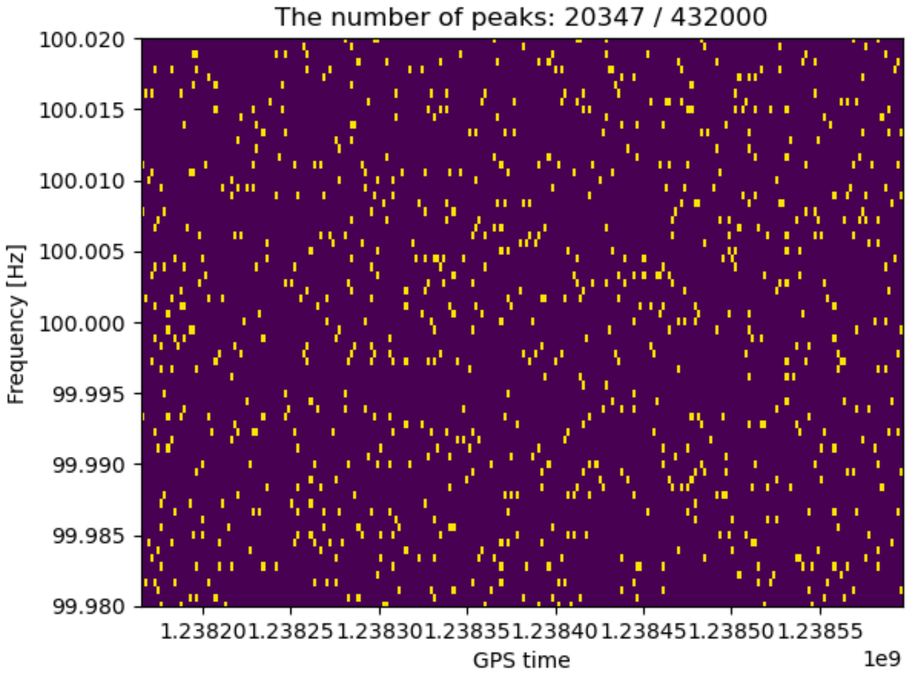

Hough transform

Assuming the relation between the input plane *M* and the parameter space *Σ*,

Hough transform converts each point in *M* into a set of points in *Σ*.

If a point in *Σ* is consistent to a point in *M*, it is incremented by one.

For each grid in *Σ*,

$$n = \sum_{i=1}^{N_{\mathrm{SFT}}} n_i \qquad n_i \in \{0, 1\}$$

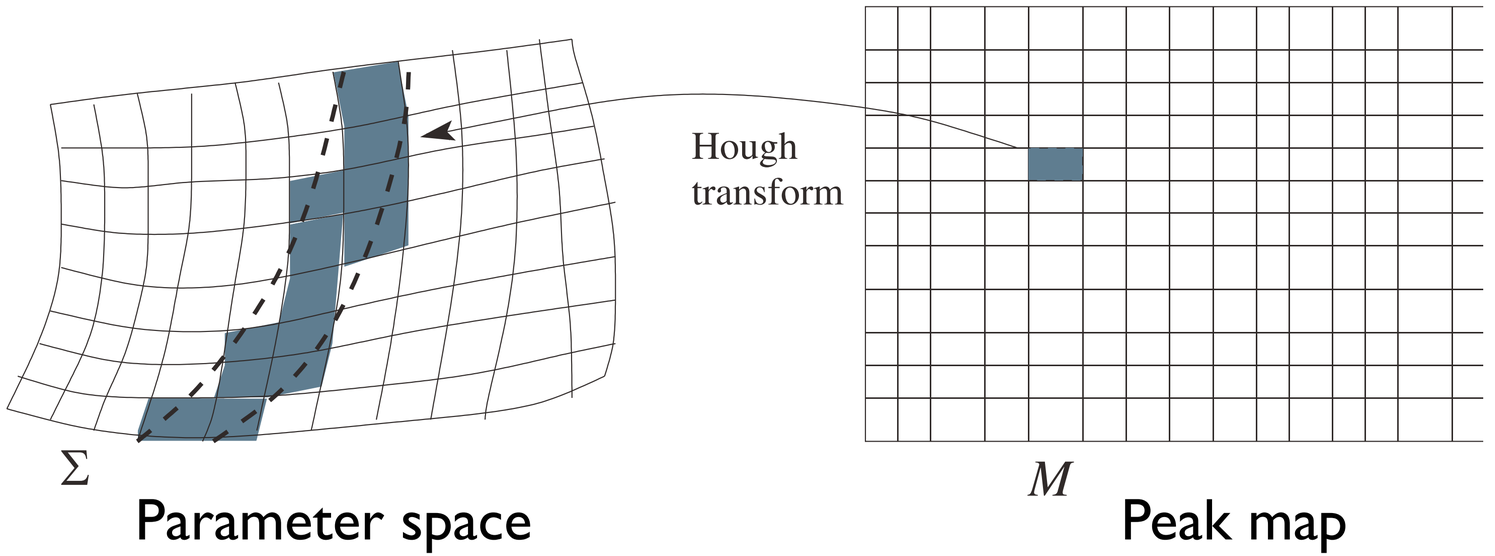

Fig: Krishnan *et al.*, PRD70, 082001

Example: linear function + noise

Data $\{(x_i, y_i)\}$ (i=1,2,…,100), $y_i = 1.0 * x_i + 0.5 + n_i$, $n_i \sim N(0,0.02)$

We assume the model $y = a * x + b$ and estimate (a, b).

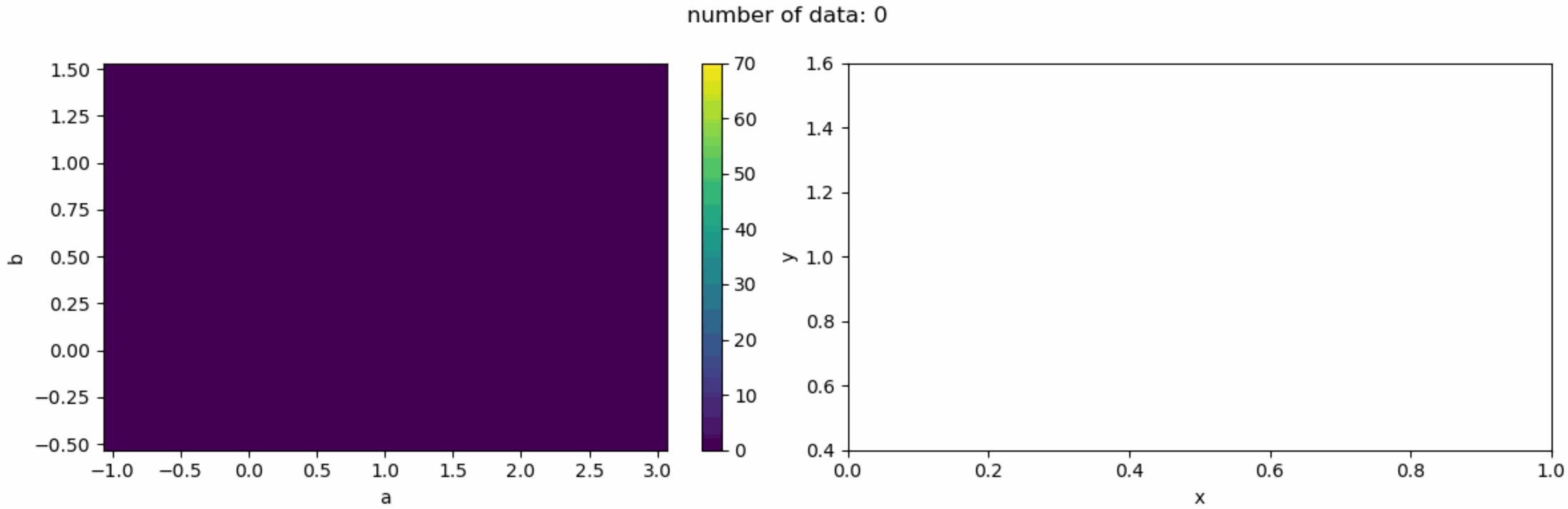

Hough map (parameter space)

Input plane

Doppler correction for peak map

For each grid on the sky, we shift the peak map to demodulate the frequency and make a Hough map. Therefore, we have a Hough map for each grid on the sky.

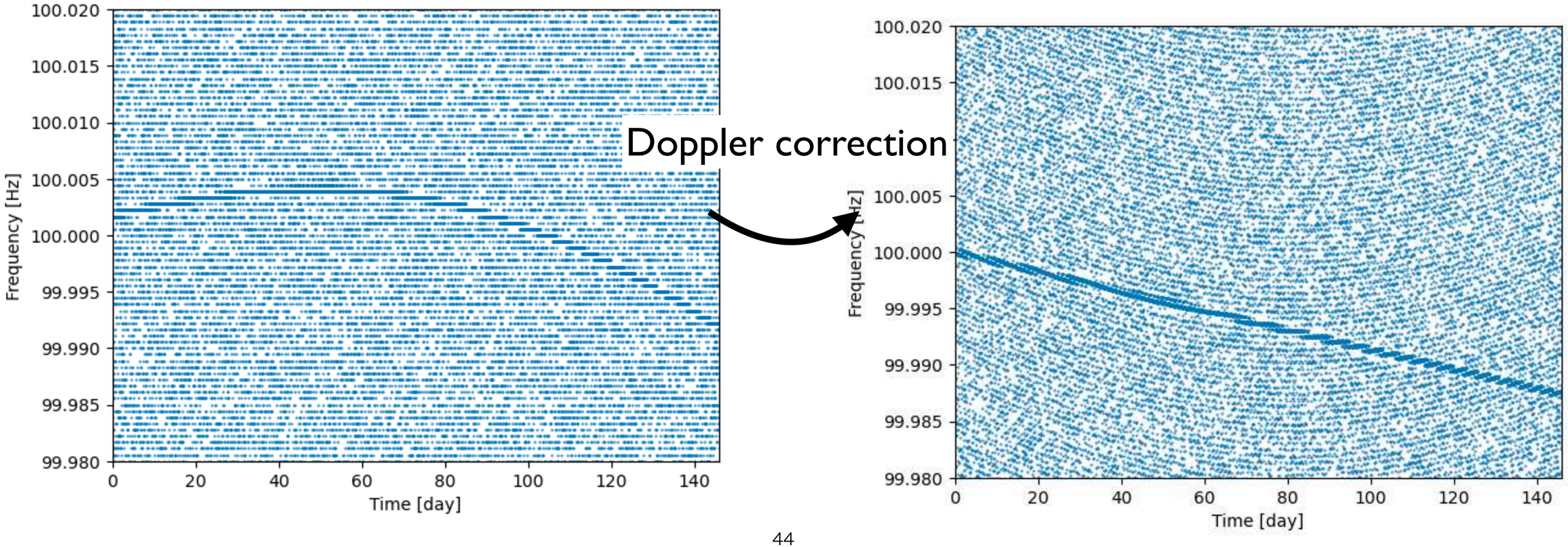

Hough map

Straight line in $(f^{(0)}, f^{(1)})$ plane

After the Doppler correction $$f = f^{(0)} + f^{(1)}(t - t_{\mathrm{ref}}) \;\Rightarrow\; f^{(1)} = -\frac{1}{t - t_{\mathrm{ref}}} f^{(0)} + \frac{f}{t - t_{\mathrm{ref}}}$$

Accounting the frequency resolution, each peak is transformed into a stripe in parameter space.

For each grid in Σ,

$$n = \sum_{i=1}^{N_{\mathrm{SFT}}} n_i \qquad n_i \in \{0, 1\}$$

Sum is taken over the frequency track consistent with the grid in Σ.

Calculating n for every grids in Σ, we get a Hough map.

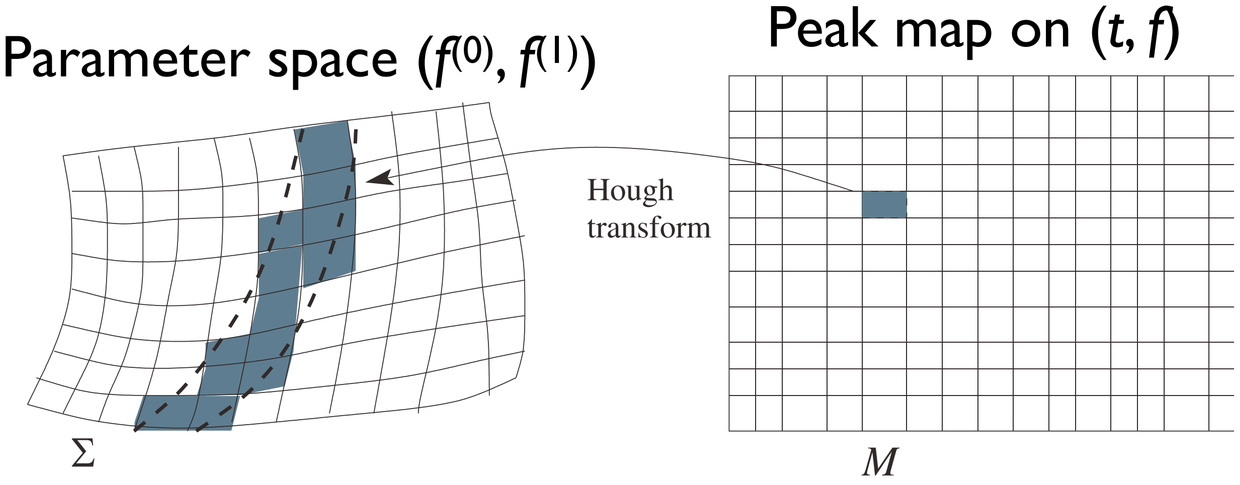

Fig: Krishnan *et al.*, PRD70, 082001

LIGO-Virgo-KAGRA Observation

From https://observing.docs.ligo.org/plan/
with some modifications

Fourth observation run (O4)

- O4 started on May 24, 2023
- Divided into three parts: O4a, O4b, O4c
- O4 concluded on November 18, 2025

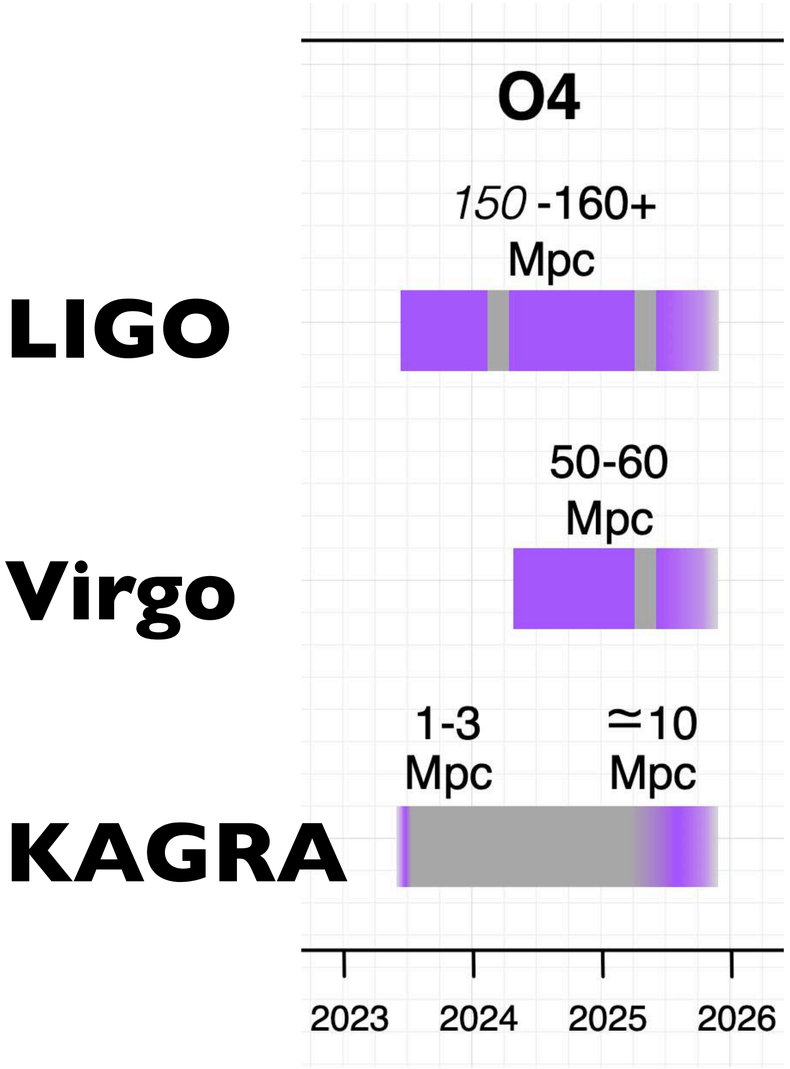

O4a Known pulsar

- Targeting 45 known pulsars
- 5-vector pipeline
- Breaking the ***spin-down limits*** for 29 targets

Spindown limits

$L_{gw} = dE_{rot}/dt$

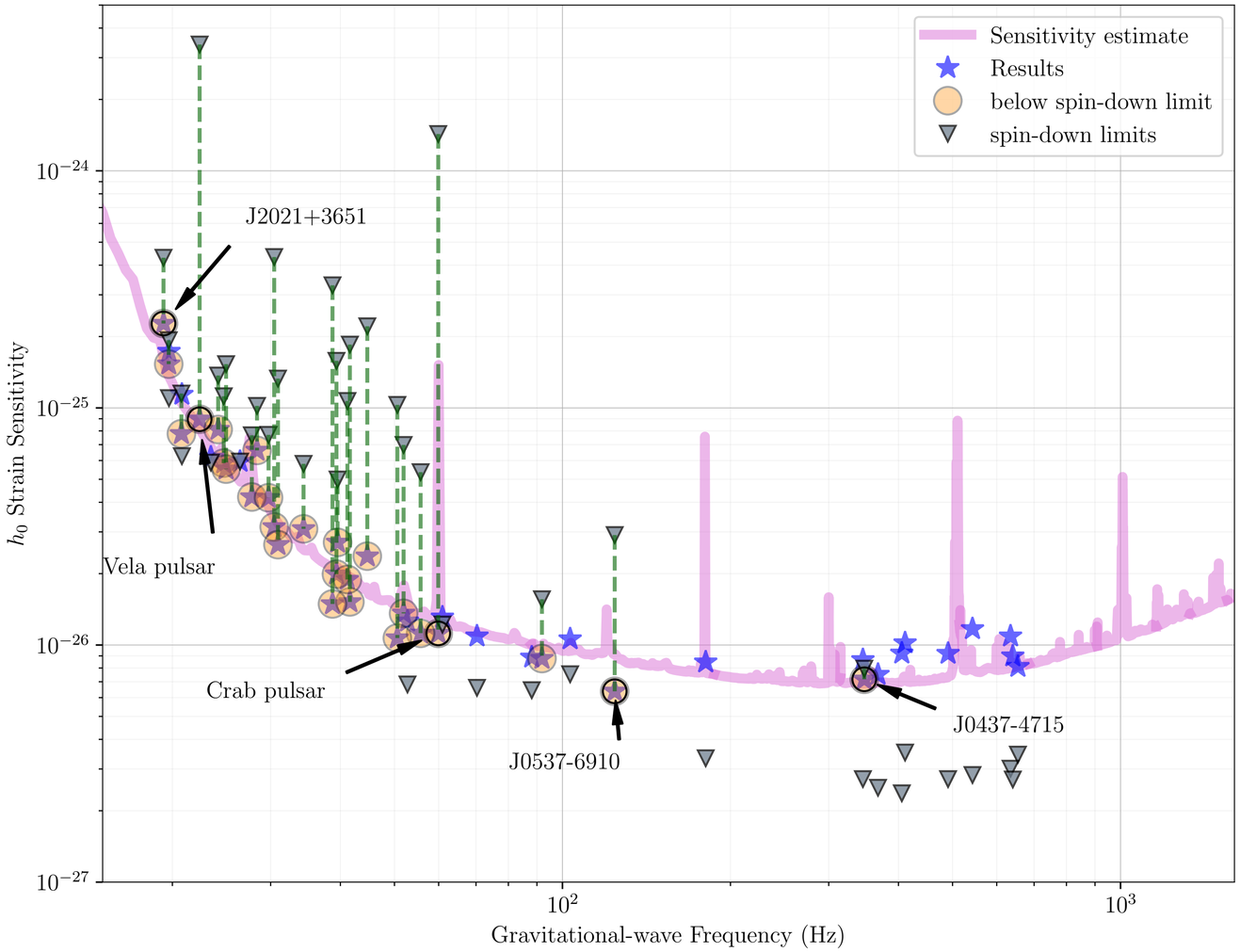

Fig: Upper limit from targeted searches (from arXiv:2501.01495)

O4a Known pulsar

$$Q_{22} = I_{zz}\epsilon\sqrt{\frac{15}{8\pi}}.$$

$$h_0 \simeq 10^{-26}\left(\frac{Q_z}{1.1\times10^{45}\ \mathrm{g\ cm^2}}\right)\left(\frac{r}{1\mathrm{kpc}}\right)^{-1} \times\left(\frac{f_{\mathrm{gw}}}{100\ \mathrm{Hz}}\right)^{2}\left(\frac{\epsilon}{10^{-6}}\right)$$

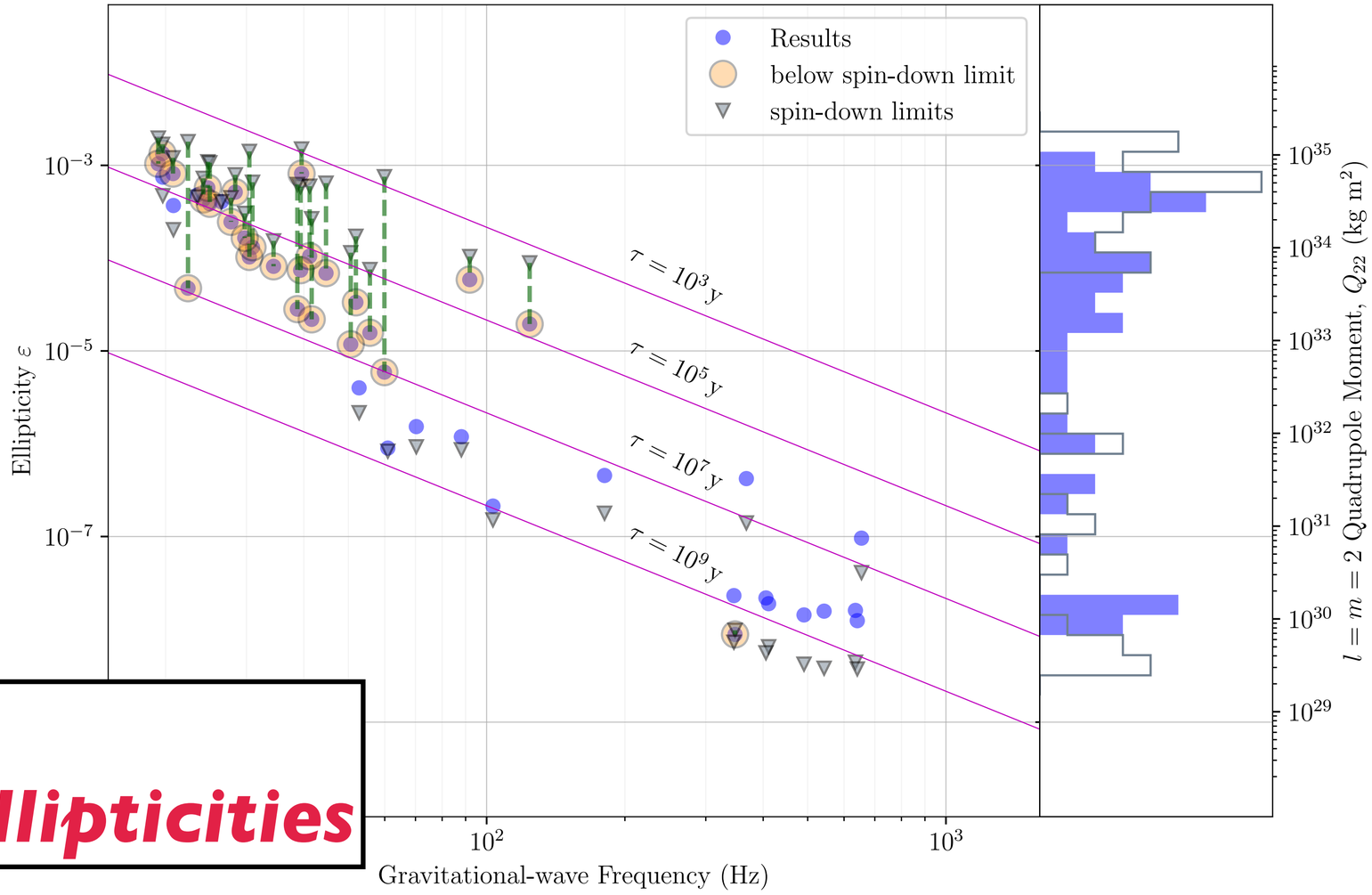

Upper limits on strain amplitudes

→ ***Constraints on the ellipticities***

Fig: Constraint on ellipticity (from arXiv:2501.01495)

O3 all-sky isolated NSs

Fig. LVK collaboration, PRD106.102008 (2022)

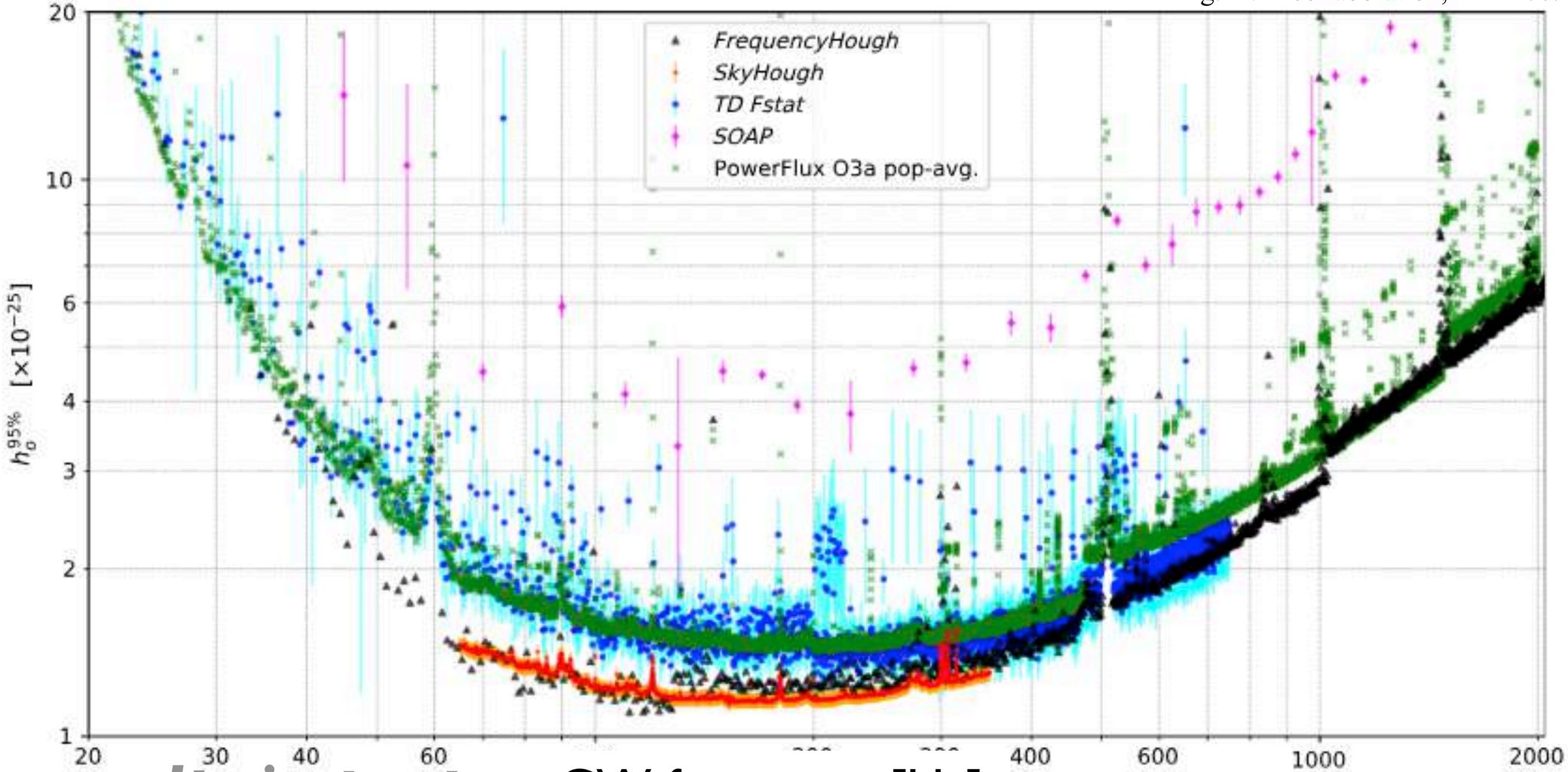

O4a results in prep.

O3 all-sky isolated NSs

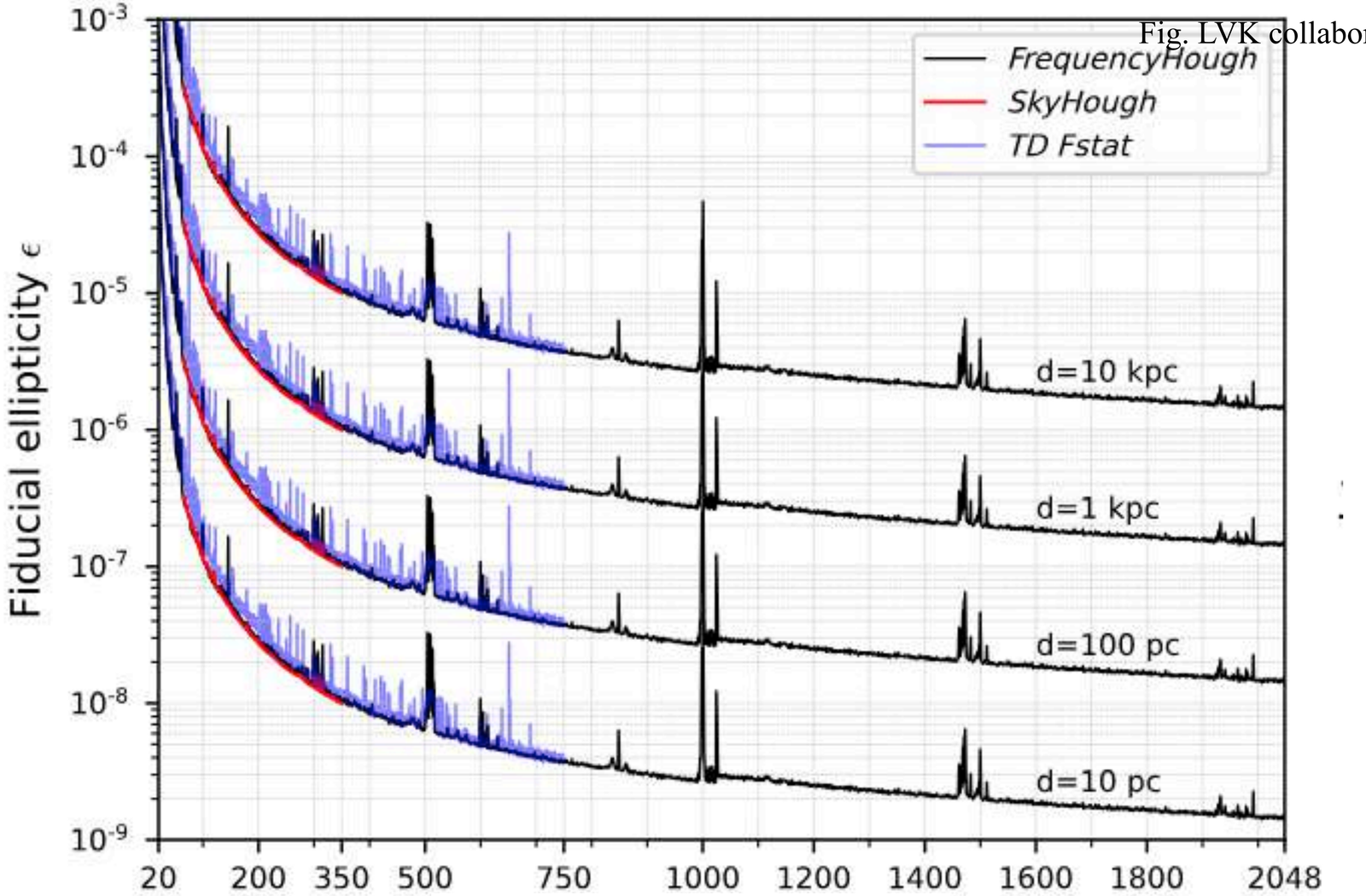

Fig. LVK collaboration, PRD106.102008 (2022)

O4a results in prep.

LIGO-Virgo-KAGRA Publications

The LIGO Scientific Collaboration and Virgo collaboration have been co-authoring observational result papers since 2010. Beginning in 2021, the KAGRA Collaboration too is co-authoring observational results from the full O3 run. See here for additional information.

BibTeX file for these papers | Click to toggle doi information | Click on any keyword to filter on that keyword | Highlighting: Event discoveries | Multi-messenger

Release Date	Title	Keywords (clear filter)	Science Summary	Journal citation	arXiv Preprint	Public Report
Dec 22, 2025 *Recent*	**Constraints on gravitational waves from the 2024 Vela pulsar glitch** (*by LSC, Virgo and KAGRA*)	O4 CW Vela LVK	summary	-	2512.17990	P2500086
Dec 18, 2025 *Recent*	**GWTC-4.0: Searches for Gravitational-Wave Lensing Signatures** (*by LSC, Virgo and KAGRA*)	O4 CBC LVK	summary	-	2512.16347	P2500419
Nov 25, 2025 *Recent*	**Search for planetary-mass ultra-compact objects using data from the first part of the LIGO-Virgo-KAGRA fourth observing run** (*by LSC, Virgo and KAGRA*)	O4 CW LVK	summary	*Submitted to PRL*	2511.19911	P2500248
Nov 21, 2025 *Recent*	**All-sky search for continuous gravitational-wave signals from unknown neutron stars in binary systems in the first part of the fourth LIGO-Virgo-KAGRA observing run** (*by LSC, Virgo and KAGRA*)	O4 CW LVK	summary	*Submitted to PRD*	2511.16863	P2500437
Nov 2, 2025	**Cosmological and High Energy Physics implications from gravitational-wave background searches in LIGO-Virgo-KAGRA's O1-O4a runs** (*by LSC, Virgo and KAGRA*)	O4 Stochastic LVK	-	*Submitted to PRX*	2510.26848	P2500150
Nov 2, 2025	**Direct multi-model dark-matter search with gravitational-wave interferometers using data from the first part of the fourth LIGO-Virgo-KAGRA observing run** (*by LSC, Virgo and KAGRA*)	O4 CW LVK	summary	*Submitted to PRL*	2510.27022	P2500252
Oct 28, 2025	**GW241011 and GW241110: Exploring Binary Formation and Fundamental Physics with Asymmetric, High-spin Black Hole Coalescences** (*by LSC, Virgo and KAGRA*)	O4 CBC LVK	summary	Astrophys. J. Lett. **993**, L21 (2025)	2510.26931	P2500402
Oct 20, 2025	**Directional search for persistent gravitational waves: Results from the first part of LIGO, Virgo, and KAGRA's fourth Observing Run** (*by LSC, Virgo and KAGRA*)	O4 Stochastic LVK	summary	*Submitted to PRD*	2510.17487	P2500380
Sep 10, 2025	**GW250114: Testing Hawking's area law and the Kerr nature of black holes** (*by LSC, Virgo and KAGRA*)	O4 CBC GW250114 LVK	summary	Phys. Rev. Lett. **135**, 111405 (2025)	2509.08054	P2500421
Sep 10, 2025	**Black Hole Spectroscopy and Tests of General Relativity with GW250114** (*by LSC, Virgo and KAGRA*)	O4 CBC GW250114 TGR LVK	summary	*Accepted by PRL*	2509.08099	P2500461
Sep 9, 2025	**GW230814: investigation of a loud gravitational-wave signal observed with a single detector** (*by A. G. Abac et al. (LSC, Virgo and KAGRA)*)	O4 GW230814 LVK	summary	*Accepted by ApJL*	2509.07348	P230814
	ultralight vector boson clouds around merger remnant and galactic black holes during the first g run (*by LSC, Virgo and KAGRA*)	O4 CW LVK	summary	*Submitted to PRD*	2509.07352	P2500256
	on rate and modified gravitational-wave propagation (*by LSC, Virgo and KAGRA*)	O4 CBC LVK	summary	*Submitted to ApJL*	2509.04348	P2400152
	ve Background from the first part of LIGO, Virgo and KAGRA's fourth Observing Run (*by LSC,*	O4 Stochastic LVK	summary	*Accepted by PRD*	2508.20721	P2500349
	ugh the first part of the fourth observing run (*by LSC, Virgo and KAGRA*)	O4 data LVK	summary	*Accepted by ApJ*	2508.18079	P2500167
	e Gravitational-Wave Transient Catalog (*by LSC, Virgo and KAGRA*)	O4 CBC GWTC LVK	summary	Astrophys. J. Lett. **995**, L18 (2025)	2508.18080	P2400293
	terizing gravitational-wave transients (*by LSC, Virgo and KAGRA*)	O4 CBC GWTC LVK	summary	*Submitted to ApJL*	2508.18081	P2400300
	ansient Catalog with Observations from the First Part of the Fourth LIGO-Virgo-KAGRA	O4 CBC GWTC LVK	summary	*Accepted by ApJL*	2508.18082	P2400386
	ompact Binaries (*by LSC, Virgo and KAGRA*)	O4 CBC LVK	summary	*Submitted to ApJL*	2508.18083	P2400004
	wave transients in the first part of the fourth LIGO-Virgo-KAGRA Observing run (*by LSC, Virgo and*	O4 Burst LVK	summary	*Accepted by PRD*	2507.12282	P2500090
	sts in the first part of the fourth LIGO-Virgo-KAGRA observing run (*by LSC, Virgo and KAGRA*)	O4 Burst LVK	summary	Phys. Rev. D **112**, 102005 (2025)	2507.12374	P2400601
	otal Mass 190-265 M_sun (*by LSC, Virgo and KAGRA*)	O4 CBC				
	n known pulsars in the first part of the fourth LIGO-Virg					
	J 2023ixf (*by LSC, Virgo and KAGRA*)	SN2023ixf	summary	Astrophys. J. **985**, 183 (2025)	2410.16565	P2400125

https://pnp.ligo.org/ppcomm/Papers.html

Summary

Summary

- CGWs will provide us with the fruitful information about astrophysics, particle physics, and cosmology.
- Searches for CGWs are challenging due to the computational cost and non-Gaussian noise.
- Various semi-coherent searches are employed to detect CGWs. F-statistic and Hough transform are powerful tools.

I didn't talk the following:

- Targeted, narrow band, and directed searches
- Sophisticated techniques (grid placement, hierarchical algorithm, etc)
- Pre-processing (gating, line cleaning, making SFT database, etc)
- Post-processing (clustering, coincidence, vetos, etc) and follow-up stage
- Many apps in lalsuite
- Machine learning & deep learning approaches

References

- Review articles (recent)
  - Sieniawska & Bejger, Universe 2019, 5(11), 217 , arXiv: 1909.12600 [CGWs and neutron stars]
  - Tenorio, Keitel & Sintes, Universe 2021, 7(12), 474 , arXiv: 2111.12575 [All-sky searches & post-processing]
  - Piccinni, Galaxies 2022, 10(3), 72 , arXiv: 2202.01088 [Sources and search results including DM candidates]
  - Wette, Astroparticle Physics 153 (2023) 102880 , arXiv: 2305.07106 [Summary of CGW search results]
  - Riles, Living Reviews in Relativity (2023) 26:3 , arXiv: 2206.06447 [Search methods for CGWs]
- Tutorials and slides
  - LIGO India Scientific Collaboration (LISC) workshop, YouTube (Jones (1, 2), Wette, Keitel)
  - PyFstat, https://github.com/PyFstat/PyFstat
  - Tutorial on Frequency Hough by Andrew Miller, https://andrew-l-miller.github.io/post/tutorial/

Backup

ex. Rotating distorted NS

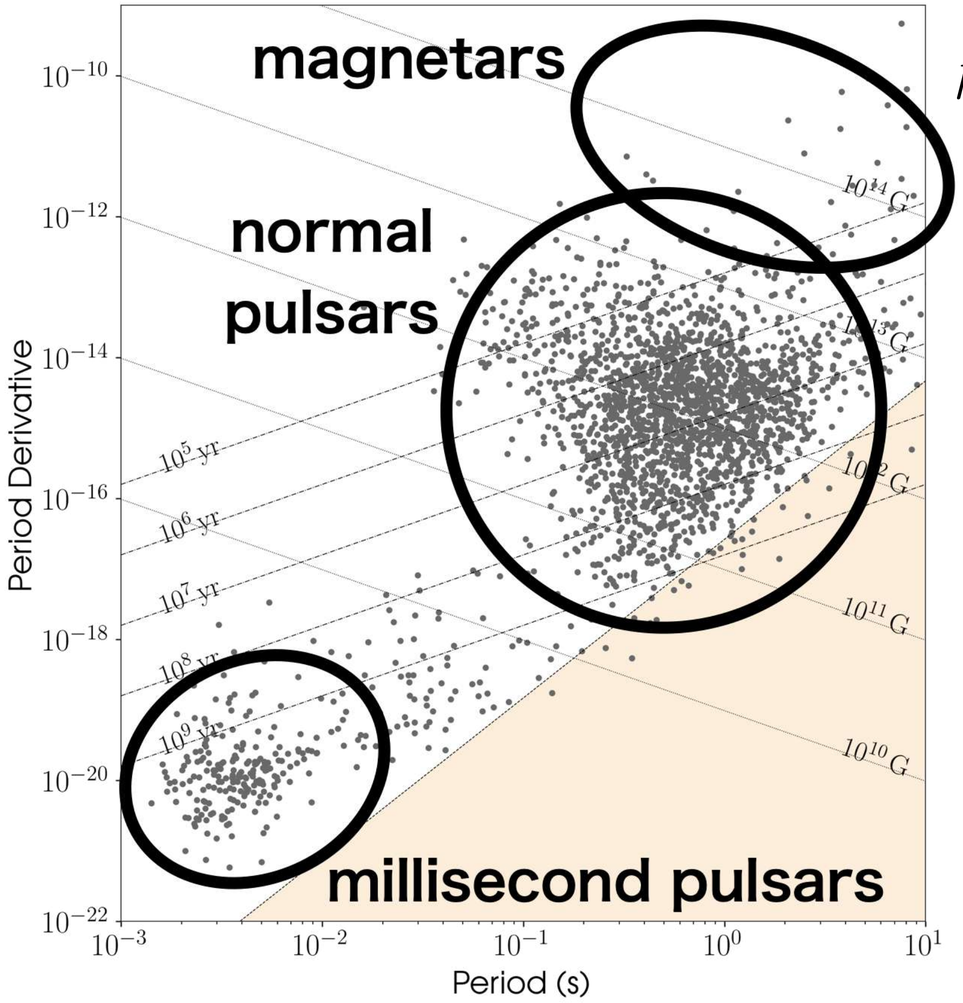

https://www.atnf.csiro.au/research/pulsar/psrcat/

Plotted by `psrqpy`

$$h_0 \simeq 10^{-26} \left(\frac{Q_z}{1.1\times 10^{45}\ \mathrm{g\ cm^2}}\right)\left(\frac{r}{1\mathrm{kpc}}\right)^{-1} \times \left(\frac{f_{\mathrm{gw}}}{100\ \mathrm{Hz}}\right)^2 \left(\frac{\epsilon}{10^{-6}}\right)$$

$$\text{ellipticity}\quad \epsilon := \frac{Q_y - Q_x}{Q_z}$$

current upper lim. ~ 2 x 10^{-25}

$$\dot{f_{\mathrm{gw}}} \sim f_{\mathrm{gw}}^2 |\dot{P}|$$

$$\sim 10^{-16}\ \mathrm{Hz/\,sec} \left(\frac{|\dot{P}|}{10^{-20}\mathrm{sec/sec}}\right)\left(\frac{f_{\mathrm{gw}}}{10^2\ \mathrm{Hz}}\right)^2$$

ex. Axion clouds around BH

Arvanitaki *et al.*, PRD 81, 123530 (2010)
Brito *et al.*, Class. Quantum Grav. 32, 134001 (2015)

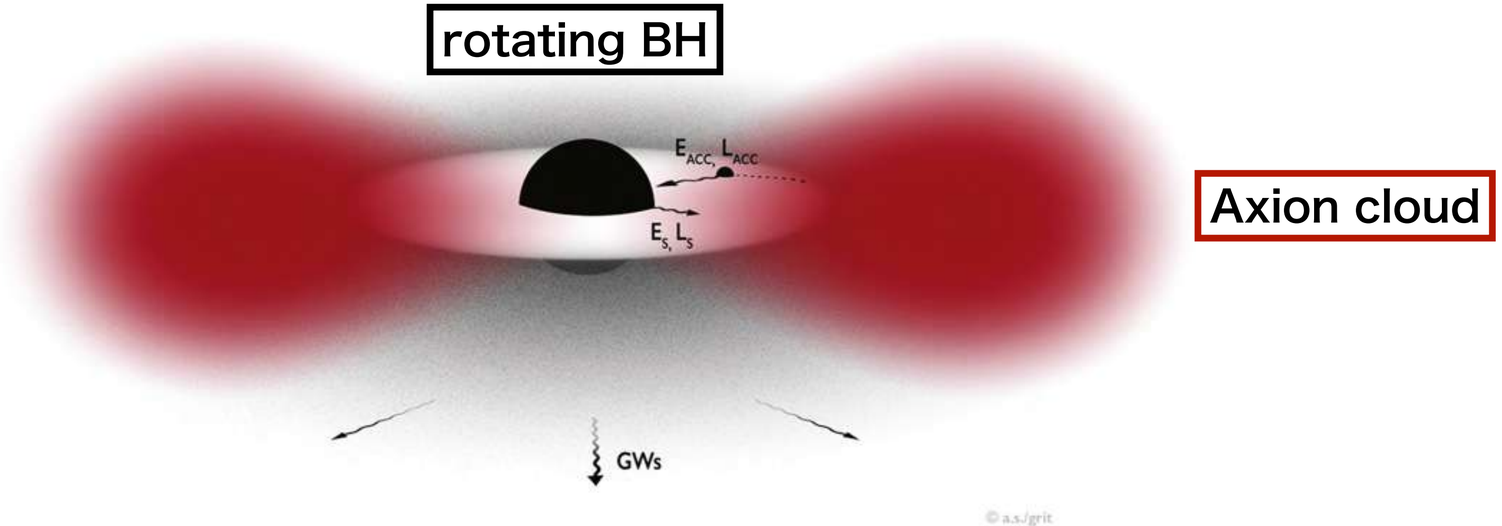

$$h_0 \sim 2.1 \times 10^{-25} \left(\frac{\alpha}{0.075}\right)^7 \left(\frac{M_{\rm BH}}{10 M_\odot}\right) \left(\frac{1{\rm kpc}}{r}\right) \qquad \alpha := \frac{R_{\rm Sch}}{\lambda_{\rm axion}}$$

$$f_{\rm gw} \sim \frac{2 m_{\rm axion} c^2}{h} \sim 2.5 \times 10^2 \ {\rm Hz} \left(\frac{m_{\rm axion}}{10^{-12} \ {\rm eV}}\right)$$

$$\tau_{\rm GW} \sim \frac{M_{\rm cloud} c^2}{\mathcal{L}_{\rm GW}} \sim 1.9 \times 10^{11} \ {\rm sec} \left(\frac{\alpha}{0.075}\right)^{-15} \left(\frac{M_{\rm BH}}{10 M_\odot}\right)$$

Sasaki *et al.*, Class. Quantum Grav. 35, 063001 (2018) as a review of PBH

ex. Small mass PBH binaries

of PBHs in our Galaxy (assuming DM consists of PBHs)

$$M_{\rm DM} \sim 1.7 \times 10^{15} M_\odot \left(\frac{R}{3{\rm Mpc}}\right)\left(\frac{v}{1500{\rm km/s}}\right)$$

$$N_{\rm PBH} \lesssim \frac{f_{\rm PBH} M_{\rm DM}}{m_{\rm PBH}} \sim 1.7 \times 10^{20} \left(\frac{m_{\rm PBH}}{10^{-6} M_\odot}\right)^{-1}$$

$$n_{\rm PBH} \lesssim \frac{N_{\rm PBH}}{R^3} \sim 6{\rm pc}^{-3}$$

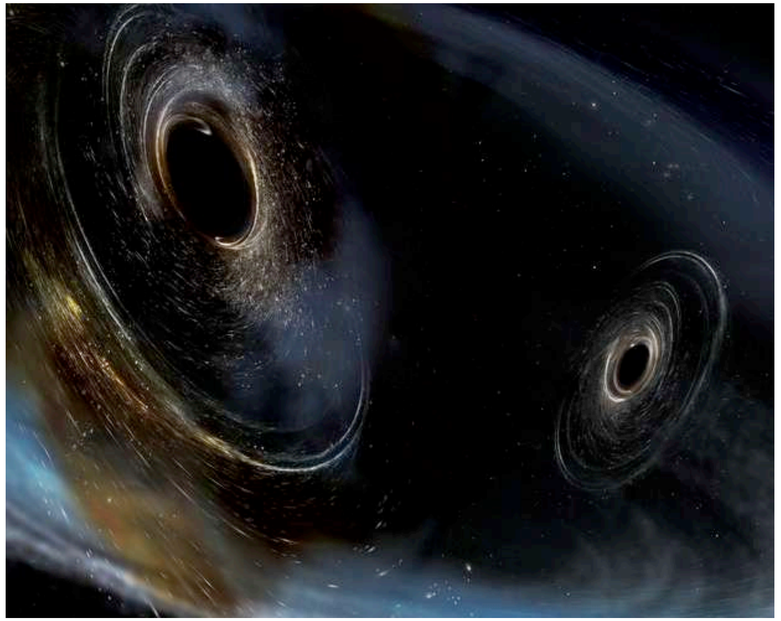

Fig: LIGO

if PBHs form a binary,

$$h_0 \sim 2 \times 10^{-25} \left(\frac{\mathcal{M}_{\rm c}}{10^{-6} M_\odot}\right)^{5/3} \left(\frac{f_{\rm gw}}{100{\rm Hz}}\right)^{2/3} \left(\frac{r}{1{\rm pc}}\right)^{-1}$$

$$\dot{f}_{\rm gw} \sim 10^{-9}\ {\rm Hz/sec} \left(\frac{\mathcal{M}_{\rm c}}{10^{-6} M_\odot}\right)^{5/3} \left(\frac{f_{\rm gw}}{100\ {\rm Hz}}\right)^{11/3}$$